

Time-dependent two-dimensional translation of a freely rotating sphere in a viscoelastic fluid


Cite as: Phys. Fluids **34**, 123110 (2022); <https://doi.org/10.1063/5.0126835>

Submitted: 17 September 2022 • Accepted: 12 November 2022 • Published Online: 14 December 2022

 Mary A. Joens,  Patrick S. Doyle,  Gareth H. McKinley, et al.

COLLECTIONS

Paper published as part of the special topic on [One Hundred Years of Giesekus](#)

 This paper was selected as Featured



View Online



Export Citation



CrossMark

ARTICLES YOU MAY BE INTERESTED IN

[English translation of Giesekus's famous article on the elasticity of liquids](#)

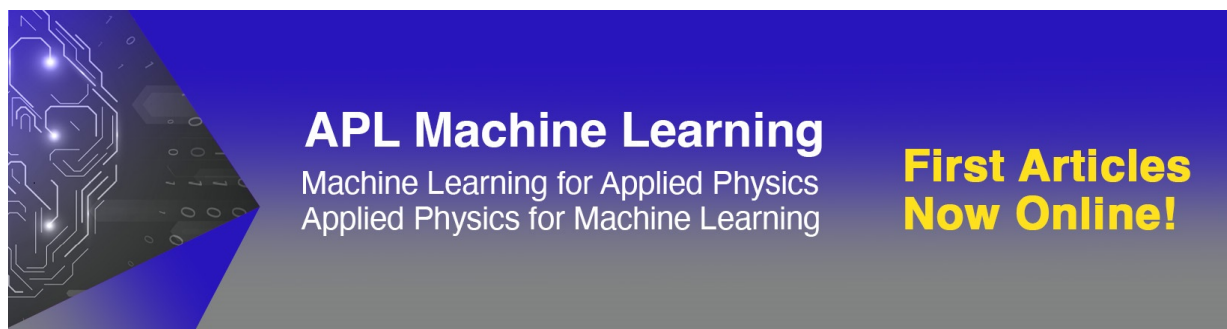
Phys. Fluids **34**, 123109 (2022); <https://doi.org/10.1063/5.0131106>

[On Oreology, the fracture and flow of “milk's favorite cookie”[®]](#)

Phys. Fluids **34**, 043107 (2022); <https://doi.org/10.1063/5.0085362>

[Kitchen flows: Making science more accessible, affordable, and curiosity driven](#)

Phys. Fluids **34**, 110401 (2022); <https://doi.org/10.1063/5.0131565>



APL Machine Learning
Machine Learning for Applied Physics
Applied Physics for Machine Learning

**First Articles
Now Online!**

Time-dependent two-dimensional translation of a freely rotating sphere in a viscoelastic fluid

Cite as: Phys. Fluids **34**, 123110 (2022); doi: [10.1063/5.0126835](https://doi.org/10.1063/5.0126835)

Submitted: 17 September 2022 · Accepted: 12 November 2022 ·

Published Online: 14 December 2022



View Online



Export Citation



CrossMark

Mary A. Joens,¹  Patrick S. Doyle,¹  Gareth H. McKinley,^{2,a)}  and James W. Swan¹ 

AFFILIATIONS

¹Department of Chemical Engineering, Massachusetts Institute of Technology, 77 Massachusetts Ave., Cambridge, Massachusetts 02139, USA

²Department of Mechanical Engineering, Massachusetts Institute of Technology, 77 Massachusetts Ave., Cambridge, Massachusetts 02139, USA

Note: This paper is part of the special topic, One Hundred Years of Giesekus.

^{a)} Author to whom correspondence should be addressed: gareth@mit.edu

ABSTRACT

This study examines the movement of a small freely rotating spherical particle in a two-dimensional trajectory through a viscoelastic fluid described by the Giesekus model. The fluid equations of motion in the inertialess limit and the Giesekus constitutive equation are expanded as a power series in the Weissenberg number, for which analytical solutions for velocity and pressure profiles at low order can be determined for the case of a steady-state flow. These steady solutions are then related to Fourier-transformed variables in frequency space through the use of correspondence relationships, allowing the analysis of time-dependent particle trajectories. The relative unsteadiness and nonlinearity of these time-dependent flows are quantified through a Deborah and Weissenberg number, respectively. The impact of changing these dimensionless parameters on the characteristics of the flow is discussed at length. We calculate the predicted rate of rotation of a small particle undergoing an arbitrary two-dimensional translation through a viscoelastic fluid, as well as the predicted correction to the force exerted on the particle arising from the interaction of particle rotation and translation. Finally, we calculate the angular velocity and total force including second-order corrections for particles executing a few specific trajectories that have been studied experimentally, as well as the predicted trajectory for a particle being directed by a known time-dependent forcing protocol.

Published under an exclusive license by AIP Publishing. <https://doi.org/10.1063/5.0126835>

I. INTRODUCTION

Understanding the movement of isolated single spheres through viscoelastic fluids is a canonical problem that has been of ongoing interest for several decades among researchers in many fields. A wide variety of both experimental and theoretical research has been conducted to advance our understanding of flows around spheres in many circumstances,^{1–4} including sedimentation,^{5,6} rotation,^{7,8} and immersion in a shear flow.^{9–11} These fundamental studies have myriad potential applications, ranging from understanding industrially relevant processes like sedimentation of spherical particles from viscoelastic matrix fluids to modeling the locomotion of microorganisms. Theoretical and numerical studies have employed a broad array of techniques; many of these studies have involved the use of a key method in our work, which is the use of asymptotic expansions to derive analytical approximations for the first corrections to the velocities, pressures, and stresses in weakly viscoelastic fluids.

Key prior studies in this field using such expansion techniques include seminal work by Hanswalter Giesekus in the 1960s,^{12,13} in which he used ordered fluid expansions of progressively higher order to

derive analytical solutions for the velocity and pressure profiles around a sphere moving steadily through a viscoelastic fluid, as well as the resulting drag force. Though previous work using such methods existed at the time, including foundational work by Leslie and Tanner,¹⁴ he was the first researcher to publish a correct result for such a calculation,¹⁵ and since his original work, many other studies have been conducted into the motion of spheres through such fluids, which rely on similar methods.¹¹ In addition to his work using ordered expansions, many subsequent researchers have used Giesekus' eponymous constitutive model to describe the rheology of the complex fluids they are studying. Originally published in 1966,¹⁶ and brought to a wider audience in 1982,¹⁷ the Giesekus model for dilute polymer solutions is one of the most widely used constitutive equations for viscoelastic liquids due to its ability to capture empirically observed phenomena like shear-thinning, non-zero normal stress differences, and bounded extensional viscosity despite its relative simplicity.¹⁸ The model has since been used to describe a variety of real fluids,^{19,20} including both the dilute polymer solutions for which it was originally formulated^{21–23} and other viscoelastic fluids like aqueous gum solutions²⁴ and blood plasma.²⁵

While the steady motion of spheres in viscoelastic fluids has been subject to extensive analytical study,^{1,2,26,27} the problem of unsteady motion has received less attention. The studies that do exist regarding unsteady motions have also largely been limited to one-dimensional movement.^{28–31} However, there are several real-world applications in which a particle is being driven in more complex trajectories by magnetic, optical, or electrical fields. These include the development of guided nano/micro-robots,^{32–34} the characterization of materials using optically or magnetically trapped particles,³⁵ and precision-controlled directed assembly of structured materials,³⁶ including applications in which these particles are immersed in viscoelastic fluids.^{37–39} Spheres being controlled by such external fields can be directed in 2D and 3D trajectories, and we will show in this study that there are several circumstances in which considering both the translational and rotational components of the flow arising from a 2D particle trajectory is necessary for obtaining a thorough understanding of relevant force–velocity or force–displacement relationships.

In this work, we derive analytical solutions for the time-dependent movement of a small, isolated, torque-free sphere through a weakly viscoelastic fluid in a trajectory that is not limited to translation in a single direction. The mathematical model for this system is described in detail in Sec. II. In Sec. III, we derive expressions for the particle rotation arising from an arbitrary movement of this type, as well as the additional corrections to the force arising from the coupling of the particle rotation with the translation in each direction of motion. We will define two dimensionless parameters, a Weissenberg number and a Deborah number, to measure the relative importance of flow nonlinearity and unsteadiness, respectively.^{40,41} The predicted correction to the force for various prescribed trajectories will be analyzed in a series of contour plots examining the relative effects of Weissenberg number, Deborah number, and the Giesekus mobility parameter α in Sec. IV. Also in Sec. IV, we will use the general solution we derive to compute the angular velocity and total force exerted on torque-free particles executing some specific trajectories of interest. We also examine the problem of predicting the trajectory of a particle in response to some externally applied force by inverting and integrating the expression for the predicted force in response to an imposed particle velocity. We will use this to examine the trajectory of a particle subjected to a specific, non-trivial time-dependent external force.

II. PROBLEM DEFINITION

A small, solid, torque-free spherical particle of radius a is submerged in an incompressible, isothermal viscoelastic fluid and subjected to an arbitrary two-dimensional, time-dependent flow at low Reynolds number ($Re = \rho V_c a / \eta_0 \ll 1$), where V_c and t_c are the characteristic velocity and time scales for the prescribed time-dependent motion. In the low-Reynolds number limit with an *a priori* unknown Strouhal number ($Sr = t_c V_c / a$), the governing equations for the system are as follows:

$$\frac{Re}{Sr} \frac{\partial \mathbf{v}(\mathbf{r}, t)}{\partial t} = -\nabla p(\mathbf{r}, t) + \beta \nabla^2 \mathbf{v}(\mathbf{r}, t) + \nabla \cdot \boldsymbol{\tau}_p(\mathbf{r}, t), \quad (1a)$$

$$\nabla \cdot \mathbf{v}(\mathbf{r}, t) = 0, \quad (1b)$$

and in order to neglect the partial time derivative of velocity, we require $Sr \gg Re$. This is a reasonable limitation to impose for this problem, as the Reynolds number and Strouhal number values for representative systems of microscale particle motion^{36,37} indicate that the

Reynolds number will almost always be significantly smaller than the Strouhal number for such flows, with typical $Re \sim 10^{-10} - 10^{-6}$ and $Sr \sim 10^{-1} - 10^2$. With this limitation met, the final momentum balance is given by

$$\beta \nabla^2 \mathbf{v}(\mathbf{r}, t) + \nabla \cdot \boldsymbol{\tau}_p(\mathbf{r}, t) - \nabla p(\mathbf{r}, t) = 0, \quad (2)$$

in which the following terms are defined: $\boldsymbol{\tau}_p(\mathbf{r}, t)$ is the polymeric stress scaled by $\eta_0 V_c / a$, where V_c is the characteristic velocity of the particle, a is the particle radius, and η_0 is the total zero-shear viscosity defined as $\eta_0 = \eta_s + \eta_p$ with η_s being the Newtonian solvent viscosity and η_p being the polymeric viscosity; $p(\mathbf{r}, t)$ is the pressure scaled by $\eta_0 V_c / a$; $\mathbf{v}(\mathbf{r}, t)$ is the velocity scaled by the characteristic velocity; and β is the dimensionless Newtonian viscosity η_s / η_0 such that $(1 - \beta) = \eta_p / \eta_0$. The position vector \mathbf{r} is centered on the particle, and the notation $|\mathbf{r}| = r$ will be used throughout. All times are scaled by a characteristic timescale t_c , whose appropriate definition will depend on the flow being considered; appropriate choices of time and velocity scales for the problems studied in this paper will be discussed later in this section.

The evolution equation for the polymeric stress in Eq. (2) must now be defined. The polymeric stress $\boldsymbol{\tau}_p$ can be described by a wide variety of constitutive models depending on the fluid behavior desired or the specific complex fluid being modeled. In this case, we will use the Giesekus model to describe the polymeric stress, which in dimensionless form can be written as

$$\boldsymbol{\tau}_p(\mathbf{r}, t) + De \frac{\partial \boldsymbol{\tau}_p(\mathbf{r}, t)}{\partial t} + Wi [\alpha (\boldsymbol{\tau}_p(\mathbf{r}, t) \cdot \boldsymbol{\tau}_p(\mathbf{r}, t)) + \mathbf{v}(\mathbf{r}, t) \cdot \nabla \boldsymbol{\tau}_p(\mathbf{r}, t) - (\nabla \mathbf{v}^T(\mathbf{r}, t) \cdot \boldsymbol{\tau}_p(\mathbf{r}, t) + \boldsymbol{\tau}_p(\mathbf{r}, t) \cdot \nabla \mathbf{v}(\mathbf{r}, t))] = 2(1 - \beta) \mathbf{e}(\mathbf{r}, t), \quad (3)$$

where $\mathbf{e}(\mathbf{r}, t) = 1/2(\nabla \mathbf{v}(\mathbf{r}, t) + \nabla \mathbf{v}^T(\mathbf{r}, t))$ and α is the dimensionless Giesekus mobility parameter quantifying the extent of shear-thinning and the magnitude of the second normal stress differences in the fluid. The Weissenberg number Wi and Deborah number De will be discussed further later in this section.

Two other key quantities of interest in this work will be the net force and the torque on the particle arising from the prescribed motion. The force exerted on the particle by the fluid is defined as

$$\mathbf{F}(t) = \int_S \mathbf{n} \cdot [p(\mathbf{r}, t) \mathbf{I} + 2\beta \mathbf{e}(\mathbf{r}, t) + \boldsymbol{\tau}_p(\mathbf{r}, t)]|_{r=1} dS, \quad (4)$$

where the surface traction is evaluated at the sphere surface, given by $r = 1$ in the dimensionless form. The torque is

$$\mathbf{T}(t) = \int_S \mathbf{r} \times [p(\mathbf{r}, t) \mathbf{I} + 2\beta \mathbf{e}(\mathbf{r}, t) + \boldsymbol{\tau}_p(\mathbf{r}, t)]|_{r=1} \cdot \mathbf{n} dS, \quad (5)$$

where in both cases dS is the surface of the spherical particle with an outward-facing normal \mathbf{n} .

With the general mathematical model established, boundary conditions for a flow with arbitrary velocities in the \mathbf{e}_1 and \mathbf{e}_2 directions are as follows:

$$\mathbf{v}(r \rightarrow \infty, t) = V_1(t) \mathbf{e}_1 + V_2(t) \mathbf{e}_2, \quad (6a)$$

$$p(r \rightarrow \infty, t) = 0, \quad (6b)$$

and the torque-free condition

$$\mathbf{T}(t) = \int_S \mathbf{r} \times [p(\mathbf{r}, t)\mathbf{I} + 2\beta\mathbf{e}(\mathbf{r}, t) + \boldsymbol{\tau}_p(\mathbf{r}, t)]|_{r=1} \cdot \mathbf{n} dS = 0, \quad (6c)$$

as well as no-slip and no-penetration conditions applied at the surface of the sphere

$$\mathbf{v}(r = 1, t) \cdot \mathbf{n} = 0, \quad (6d)$$

$$\mathbf{v}(r = 1, t) = \boldsymbol{\Omega}(t) \times \mathbf{n}. \quad (6e)$$

In this case, the frame of reference is centered on the particle, so the velocity boundary conditions are applied at $r \rightarrow \infty$. For the equivalent problem of a particle moving through a quiescent fluid, the velocity boundary conditions in Eq. (6a) would be opposite in sign and applied at the surface, resulting in a velocity $\tilde{\mathbf{v}}(\mathbf{r}, t) = \mathbf{v}(\mathbf{r}, t) - \mathbf{v}_\infty$ instead. In the case we are working with, in which the frame of reference is centered on the particle, the far-field, imposed velocity consists in general of components in both the \mathbf{e}_1 and \mathbf{e}_2 directions, with time variations described by $V_1(t)$ and $V_2(t)$, respectively. So, for example, in the circular particle trajectory shown in 1(a), the particle’s velocity will be the derivative of its position, and as it is moving through a quiescent fluid, the appropriate boundary conditions would be

$$\begin{aligned} V_1(r \rightarrow \infty) &= 2\pi fR \sin(2\pi ft), \\ V_2(r \rightarrow \infty) &= -2\pi fR \cos(2\pi ft), \end{aligned} \quad (7)$$

and the torque-free condition described in Eq. (6c) gives rise to the rotation described in Eq. (6e), described by some time-dependent angular velocity term $\boldsymbol{\Omega}(t)$, which must be calculated based on the interaction of the two imposed flow fields.

In this initial formulation, we have explicitly included the argument for each term, for example, writing $\boldsymbol{\tau}_p(\mathbf{r}, t)$, $\mathbf{v}(\mathbf{r}, t)$, $p(\mathbf{r}, t)$ to emphasize that these are time-dependent quantities. However, for the sake of brevity and compactness of equations, throughout the rest of this work we will not do so, and variables with no diacritical mark above them should be understood to be time- and space-dependent. When terms with different arguments are introduced, for example, the frequency-dependent term $\hat{\mathbf{v}}(\mathbf{r}, \omega)$, the arguments will again initially be included and clearly described in the text in their first instance, and they will then be indicated by the corresponding diacritical mark going forward.

In the above equations and throughout, Wi and De refer to the Weissenberg and Deborah numbers, respectively, which have the following definitions:

$$De = \frac{\lambda}{t_c} \quad Wi = \frac{\lambda V_c}{a}, \quad (8)$$

where λ is the single characteristic relaxation time of the Giesekus model describing the viscoelastic fluid. The Weissenberg number Wi provides a relative measure of the magnitude of the nonlinear elastic and viscous forces in the fluid, and De is a measure of the flow unsteadiness, defined as a ratio of the relaxation time of the fluid to a representative process timescale t_c , which we define as the timescale on which the flow is changing; V_c is defined as the maximum absolute value of the far-field velocity field $\mathbf{V}(r \rightarrow \infty, t)$.

For example, we consider a circular trajectory as shown in Fig. 1(a), where the frequency of the particle motion is $2\pi f$ and the radius of the circular trajectory is R . In this case, an appropriate choice of V_c would be $V_c = 2\pi fR$, and $t_c = 1/(2\pi f)$ may be chosen

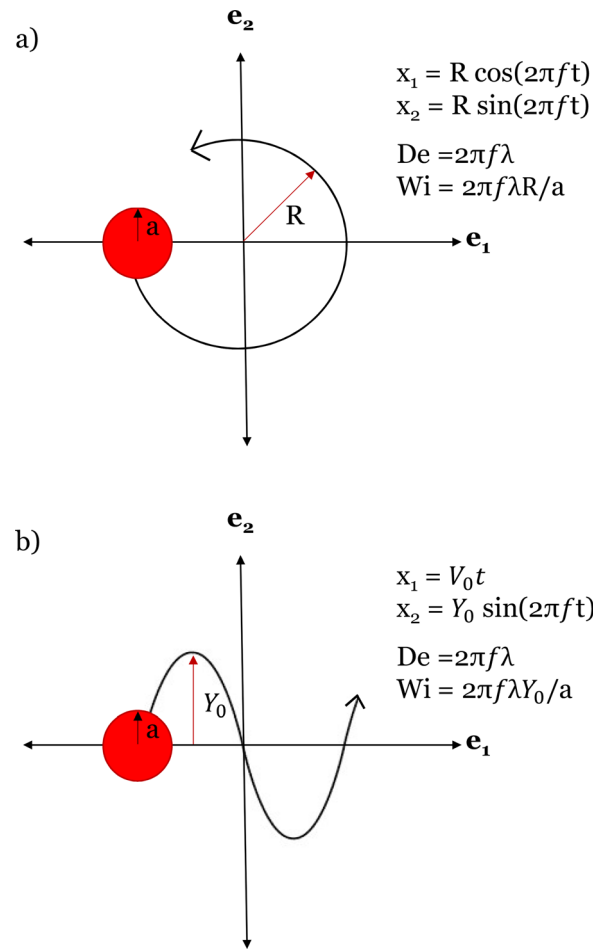


FIG. 1. A wide variety of 2D particle trajectories can be analyzed using the solutions derived in this work, including (a) a particle moving in a circle with some known radius R , and (b) a particle moving in a sinusoidal pattern with a displacement Y_0 .

as an appropriate timescale. In this case, $De = 2\pi f\lambda$ and $Wi = 2\pi f\lambda R/a = De(R/a)$. For the sinusoidal trajectory shown in Fig. 1(b), the characteristic timescale t_c would again be $t_c = 1/(2\pi f)$, and an appropriate velocity scale may be $V_c = 2\pi fY_0$. These two forms lead to an essentially identical definition of the Weissenberg and Deborah numbers as in the case of a circular trajectory, with the trajectory radius R for the circular case instead replaced by the amplitude Y_0 for the case of an oscillatory sinusoidal trajectory as shown in Fig. 1(b).

We can once again closely consider the case of the circular trajectory in Fig. 1 in order to better understand the interplay of the Weissenberg number, Deborah number, and the ratio of the particle radius to the trajectory radius, a/R , which we will henceforth refer to as the “radius ratio” (when referring to the ratio R/a , we will use the term “inverse radius ratio”). Figure 2 shows an operating space in which the solutions derived in this work are valid. As indicated by the green arrows at the center of the diagram, increasing the Weissenberg number increases nonlinearity, while increasing the Deborah number (moving along the diagonal of this figure) increases unsteadiness.

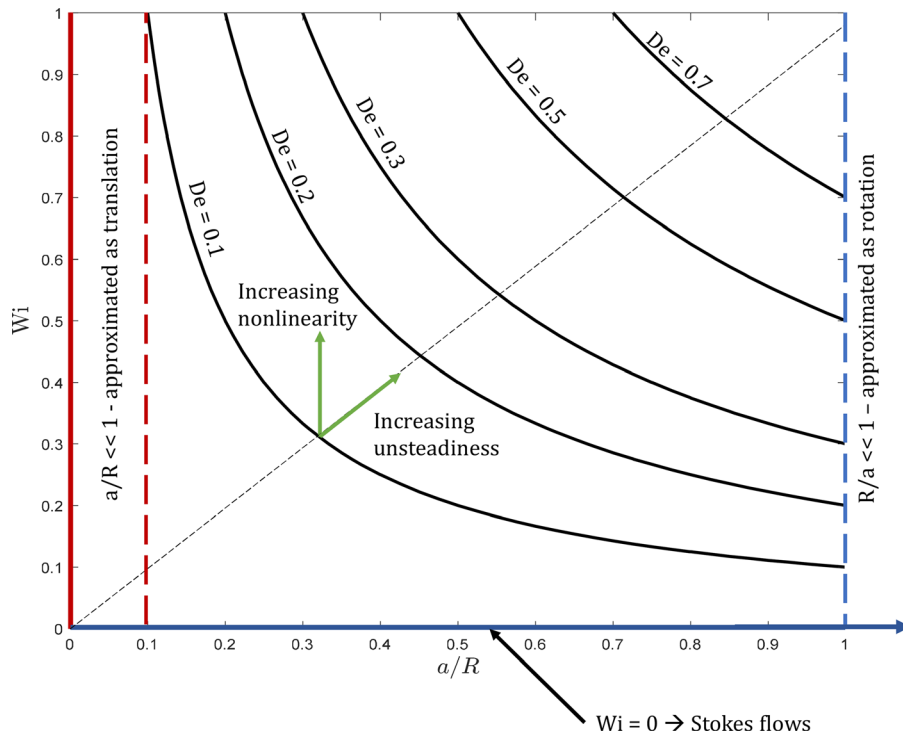


FIG. 2. The accessible “operating space” for describing a particle moving in a circular trajectory using the methods outlined in this work is shown as a function of dimensionless parameters Wi , De , and the radius ratio a/R . The red dashed line on the left indicates the limit in which these flows can be approximated a simple 1D translation through an elastic fluid, and the blue dashed line on the right indicates where they can be approximated as simple rotation.

As such, the x axis of this figure—the case of $Wi = 0$, or full linearity—represents Stokes flows of Newtonian fluids. Conversely, the y axis represents the case of increasing nonlinearity in the limit of the radius ratio $a/R \rightarrow 0$, meaning that the radius of the trajectory is far greater than the radius of the particle. This case is asymptotically equivalent to that of a one-dimensional translation through a viscoelastic fluid, which has been studied previously.^{6,31} Similarly, as indicated by the dashed line at a radius ratio of $a/R = 1$, once the radius of the trajectory is the same as, or smaller than, the particle radius ($a/R > 1$), the motion overall can be increasingly well approximated as simple particle rotation in a viscoelastic fluid.⁷ However, moving away from either axis into the central portion of the figure introduces both fluid nonlinearity and flow unsteadiness, and both particle rotation and translation as well as their coupling must be considered in this region to fully characterize the flow.

In Sec. III, we will derive the rate of particle rotation and the leading-order force correction arising from rotation–translation coupling very generally for an arbitrary particle velocity. However, we will return to the example of a circular trajectory in Sec. IV and more closely examine the interplay of the fluid nonlinearity and flow unsteadiness described by the Weissenberg and Deborah numbers.

III. SOLUTION METHODS

To evaluate general solutions to this class of problems for 2D motions of spherical particles through viscoelastic fluids, we make use of techniques developed in our previous work analyzing the unsteady motion of particles in a simpler 1D trajectory.³¹ In brief,

we use an asymptotic expansion of the governing equations in powers of the Weissenberg number. We then use correspondence relationships to connect the steady-state solutions of the equations at various orders to the frequency-dependent solutions at those orders, and then use the Lorentz reciprocal theorem⁴² to calculate the integrated force and torque at higher orders using only information from lower-order solutions. The final solution at each order will include an expression for the angular velocity of a particle undergoing an arbitrary 2D translation and the correction to the force as a function of the Weissenberg and Deborah numbers exerted on the particle arising from the coupling of this rotation with the particle’s translation.

We write the asymptotic expansion quite generally as

$$\mathbf{X} = \sum_{n=0}^{\infty} Wi^n \mathbf{X}^{(n)}, \tag{9a}$$

$$\mathbf{X} = \mathbf{X}^{(0)} + Wi\mathbf{X}^{(1)} + Wi^2\mathbf{X}^{(2)} + \dots \tag{9b}$$

where \mathbf{X} represents the variables in the problem: \mathbf{v} , p , $\boldsymbol{\tau}_p$, \mathbf{e} , \mathbf{F} , and T . It is worth noting here that throughout the text, the term “leading order” will be used to describe terms of $\mathcal{O}(1)$, or $\mathcal{O}(Wi^0)$, “first order” is used to indicate the first correction appearing at $\mathcal{O}(Wi)$, etc.

We can now formulate the governing equations at each order in the expansion

$$\beta \nabla^2 \mathbf{v}^{(n)} + \nabla \cdot \boldsymbol{\tau}_p^{(n)} + \nabla p^{(n)} = 0, \tag{10a}$$

$$\nabla \cdot \mathbf{v}^{(n)} = 0, \tag{10b}$$

as well as the constitutive equation

$$\begin{aligned} \boldsymbol{\tau}_p^{(n)} + \text{De} \frac{\partial \boldsymbol{\tau}_p^{(n)}}{\partial t} + \sum_{m=1}^{n-1} \left[\alpha (\boldsymbol{\tau}_p^{(n-m)} \cdot \boldsymbol{\tau}_p^{(m)}) + \boldsymbol{v}^{(n-m)} \cdot \nabla \boldsymbol{\tau}_p^{(m)} \right. \\ \left. - (\nabla \boldsymbol{v}^{(n-m)T} \cdot \boldsymbol{\tau}_p^{(m)} + \boldsymbol{\tau}_p^{(m)} \cdot \nabla \boldsymbol{v}^{(n-m)T}) \right] = 2(1 - \beta) \boldsymbol{e}^{(n)}, \end{aligned} \quad (11)$$

where the summation term is used to collect all of the combinations of terms that result in total order n for $n \leq 3$.

In addition to the general, time-dependent equations, we will also be particularly interested in two specific cases of this problem: at steady state, and in the frequency domain. In both of these cases, the governing equations and boundary conditions will be formally the same as in the time-dependent case, though the polymeric stress will change depending on the case in question. Going forward, steady-state variables will be indicated with a tilde [e.g., $\tilde{\boldsymbol{\tau}}_p(\mathbf{r})$], and the corresponding frequency-dependent ones with a caret [e.g., $\hat{\boldsymbol{\tau}}_p(\mathbf{r}, \omega)$]. In the steady-state case, the polymeric stress is

$$\begin{aligned} \tilde{\boldsymbol{\tau}}_p^{(n)}(\mathbf{r}) + \sum_{m=1}^{n-1} \left[\alpha (\tilde{\boldsymbol{\tau}}_p^{(n-m)}(\mathbf{r}) \cdot \tilde{\boldsymbol{\tau}}_p^{(m)}(\mathbf{r})) + \tilde{\boldsymbol{v}}^{(n-m)}(\mathbf{r}) \cdot \nabla \tilde{\boldsymbol{\tau}}_p^{(m)}(\mathbf{r}) \right. \\ \left. - (\nabla \tilde{\boldsymbol{v}}^{(n-m)T}(\mathbf{r}) \cdot \tilde{\boldsymbol{\tau}}_p^{(m)}(\mathbf{r}) + \tilde{\boldsymbol{\tau}}_p^{(m)}(\mathbf{r}) \cdot \nabla \tilde{\boldsymbol{v}}^{(n-m)}(\mathbf{r})) \right] = 2(1 - \beta) \tilde{\boldsymbol{e}}^{(n)}. \end{aligned} \quad (12)$$

Frequency-dependent variables are defined as the Fourier transform of their time-dependent counterparts. For any variable \mathbf{X} , the relationship between time-dependent and frequency-dependent quantities is

$$\hat{\mathbf{X}}(\omega) = \mathcal{F}[\mathbf{X}(t)] = \int_{-\infty}^{\infty} \mathbf{X}(t) e^{-i\omega t} dt, \quad (13)$$

and so, in the frequency-dependent case, the polymeric stress is

$$\begin{aligned} \hat{\boldsymbol{\tau}}_p^{(n)}(\mathbf{r}, \omega) = \chi(\omega) \left(2(1 - \beta) \hat{\boldsymbol{e}}^{(n)}(\mathbf{r}, \omega) \right. \\ \left. - \sum_{m=1}^{n-1} \left[\alpha (\hat{\boldsymbol{\tau}}_p^{(n-m)}(\mathbf{r}, \omega) * \hat{\boldsymbol{\tau}}_p^{(m)}(\mathbf{r}, \omega)) \right. \right. \\ \left. \left. + \hat{\boldsymbol{v}}^{(n-m)}(\mathbf{r}, \omega) * \nabla \hat{\boldsymbol{\tau}}_p^{(m)}(\mathbf{r}, \omega) \right. \right. \\ \left. \left. - (\nabla \hat{\boldsymbol{v}}^{(n-m)T}(\mathbf{r}, \omega) * \hat{\boldsymbol{\tau}}_p^{(m)}(\mathbf{r}, \omega) \right. \right. \\ \left. \left. + \hat{\boldsymbol{\tau}}_p^{(m)}(\mathbf{r}, \omega) * \nabla \hat{\boldsymbol{v}}^{(n-m)}(\mathbf{r}, \omega)) \right] \right), \end{aligned} \quad (14)$$

where the term $\chi(\omega) = 1/(1 + i\omega\text{De})$ scales the polymeric contribution to the complex viscosity, and the symbol $*$ denotes a convolution of two terms. Moving forward, the calculations performed will primarily involve the frequency-space terms, and we will once again begin omitting explicit indications of the appropriate arguments for each variable and denoting their time or frequency dependence only by their respective diacritical marks (carets for frequency-dependent terms) or lack thereof (for time-dependent terms).

A. Leading-order solution

We proceed with our calculations in terms of the frequency-dependent variables due to their greater convenience for analyzing time-dependent quantities. At $\mathcal{O}(1)$, or leading order, we recover the Stokes solution, whose governing equations in frequency space are

$$\beta \nabla^2 \hat{\boldsymbol{v}}^{(0)} + \nabla \cdot \hat{\boldsymbol{\tau}}_p^{(0)} - \nabla \hat{p}^{(0)} = 0, \quad (15a)$$

$$\nabla \cdot \hat{\boldsymbol{v}}^{(0)} = 0, \quad (15b)$$

and the constitutive equation is

$$\hat{\boldsymbol{\tau}}_p^{(0)} = 2\chi(\omega)(1 - \beta)\hat{\boldsymbol{e}}^{(0)}, \quad (16)$$

and finally, the boundary conditions are

$$\hat{\boldsymbol{v}}^{(0)}(r \rightarrow \infty) = \hat{V}_1(\omega)\mathbf{e}_1 + \hat{V}_2(\omega)\mathbf{e}_2, \quad (17a)$$

$$\hat{\boldsymbol{v}}^{(0)}(r = 1) = \hat{\Omega}(\omega)\mathbf{e}_3, \quad (17b)$$

$$\hat{p}^{(0)}(r \rightarrow \infty) = 0, \quad (17c)$$

and the torque-free condition

$$\int_S \mathbf{r} \times \left[\hat{p}^{(0)}\mathbf{I} + 2\beta\hat{\boldsymbol{e}} + \hat{\boldsymbol{\tau}}_p^{(0)} \right] \Big|_{r=1} \cdot \mathbf{n} dS = 0, \quad (17d)$$

where $\hat{V}_1(\omega) = \mathcal{F}[V_1(t)]$, $\hat{V}_2(\omega) = \mathcal{F}[V_2(t)]$, and $\hat{\Omega}(\omega) = \mathcal{F}[\Omega(t)]$, with $\mathcal{F}[*]$ indicating a Fourier transform.

The frequency-space variables in these equations can be related to their steady-state counterparts by application of a correspondence relationship.⁴³ However, the multi-directional aspect of this particular flow requires additional notation to indicate which components of the flow are related to which imposed flow direction. For example, at leading order, we can write $\hat{\boldsymbol{v}}^{(0)} = \hat{\boldsymbol{v}}_1^{(0)} + \hat{\boldsymbol{v}}_2^{(0)}$ where $\hat{\boldsymbol{v}}_1^{(0)}$ is the velocity contribution driven by the imposed flow in the \mathbf{e}_1 direction, and $\hat{\boldsymbol{v}}_2^{(0)}$ is the contribution driven by the imposed flow in the \mathbf{e}_2 direction. The same convention applies to both steady-state and frequency-space variables. At higher orders, at which point coupling of flow fields gives rise to variables with contributions arising from multiple flow directions, additional subscripts would be needed (e.g., $\hat{\boldsymbol{\tau}}_{p,1,2}$ indicating a stress component impacted by both velocities directed in the \mathbf{e}_1 and \mathbf{e}_2 directions). With this in hand, we can establish the leading-order correspondence relationships

$$\hat{\boldsymbol{v}}_i^{(0)} = \hat{V}_i(\omega)\hat{\boldsymbol{v}}_i^{(0)}, \quad (18a)$$

$$\hat{p}_i^{(0)} = \hat{V}_i(\omega)\eta^*(\omega)\hat{p}_i^{(0)}, \quad (18b)$$

$$\hat{\boldsymbol{\tau}}_{p,i}^{(0)} = \hat{V}_i(\omega)\chi(\omega)\hat{\boldsymbol{\tau}}_{p,i}^{(0)}, \quad (18c)$$

where $i = \{1, 2, 3\}$, indicating terms governed by each of the flow directions. The term $\eta^*(\omega)$ is the complex viscosity of the fluid, defined as $\beta + (1 - \beta)\chi(\omega) = \eta^*(\omega)$, where again $\chi(\omega) = 1/(1 + i\omega\text{De})$.

The steady-state solutions for the velocity and pressure profiles in dimensionless form at leading order [i.e., $\mathcal{O}(\text{Wi}^0)$] are the well-known solutions for flow of a Newtonian fluid around a sphere⁴⁴

$$\tilde{\boldsymbol{v}}_i^{(0)}(\mathbf{r}) = V_j - \left[\frac{3}{4r} \left(\delta_{ij} + \frac{r_i r_j}{r^2} \right) + \frac{1}{4r^3} \left(\delta_{ij} - \frac{3r_i r_j}{r^2} \right) \right] V_j, \quad (19a)$$

$$\tilde{p}_i^{(0)}(\mathbf{r}) = \frac{3r_j}{2r^3} V_j, \quad (19b)$$

where $j = \{1, 2\}$ and V_j is thus the imposed velocity in the \mathbf{e}_1 and \mathbf{e}_2 directions. The velocities in each direction are, at this order, superimposed and non-interacting. Finally, the dimensionless, frequency-dependent force at this order is simply

$$\hat{\mathbf{F}}^{(0)}(\omega) = 6\pi\eta^*(\omega)(\hat{V}_1(\omega)\mathbf{e}_1 + \hat{V}_2(\omega)\mathbf{e}_2). \quad (20)$$

As will be the case throughout this work, if the time-dependent force is the desired quantity, one can simply take the inverse Fourier transform of this frequency-dependent solution. The inverse Fourier transform of a transformed variable $\hat{f}(\omega)$ is given by

$$f(t) = \frac{1}{2\pi} \int_{-\infty}^{\infty} \hat{f}(\omega)e^{i\omega t} d\omega, \quad (21)$$

and we will use this formulation of the time-dependent force to analyze some specific flows in Sec. IV.

B. Calculation of angular velocity

While the velocity fields at leading order are superimposable and non-interacting, at higher orders this is no longer true, and they can couple and give rise to a net particle rotation. We can calculate this rotation by first determining the torque on the particle that would arise at order $\mathcal{O}(\text{Wi})$ from the interactions of the $\mathcal{O}(1)$ flow fields generated by movement in the \mathbf{e}_1 and \mathbf{e}_2 directions with each other. Since the particle is torque-free, this must be exactly balanced by its rotation.

We can use the Lorentz reciprocal theorem to formulate an expression that allows us to calculate the torque on the particle arising at $\mathcal{O}(\text{Wi})$ using only $\mathcal{O}(1)$ terms. We do this by first defining an arbitrary auxiliary flow $\hat{\mathbf{v}}'$ with a pressure profile \hat{p}' . This flow will have the boundary conditions $\hat{\mathbf{v}}'(r=1) = \boldsymbol{\Omega}' \times \mathbf{r} = \mathbf{U}'$, $\hat{\mathbf{v}}'(r \rightarrow \infty) = 0$, $\hat{p}'(r \rightarrow \infty) = 0$. The deviatoric stress in this flow is $\hat{\boldsymbol{\tau}}' = 2\eta^*(\omega)\mathbf{e}'$, where $\eta^*(\omega)$ is the complex viscosity normalized by the total zero-shear viscosity. The rate of strain is $\mathbf{e}' = \boldsymbol{\Omega}' \cdot \mathbf{S}(\mathbf{r})$, where $\mathbf{S}(\mathbf{r})$ is a third rank tensor known from the solution for simple rotation of a particle in a Newtonian fluid

$$S_{ijk}(\mathbf{r}) = \frac{-3}{r^5} (\varepsilon_{ikm}r_m r_j + \varepsilon_{jkm}r_m r_i), \quad (22)$$

where ε_{ijk} is the Levi-Civita alternating symbol.¹⁸ We can then calculate the torque by constructing a standard reciprocal theorem argument

$$\begin{aligned} \int_V \nabla \cdot [(-\hat{p}'\mathbf{I} + 2\beta\hat{\mathbf{e}}^{(1)} + \hat{\boldsymbol{\tau}}_p^{(1)}) \cdot \hat{\mathbf{v}}' d\mathbf{r} \\ = \int_V \nabla \cdot [(-\hat{p}'\mathbf{I} + \boldsymbol{\tau}') \cdot \hat{\mathbf{v}}^{(1)} d\mathbf{r}, \end{aligned} \quad (23)$$

with V indicating the volume of fluid around the particle. Some rearrangement of terms, application of the divergence theorem, and several algebraic steps result in a fairly simple expression for the torque

$$\mathbf{T}^{(1)} = \int_V \mathbf{S}(\mathbf{r}) : (\hat{\boldsymbol{\tau}}_p^{(1)} - 2\chi(\omega)\hat{\mathbf{e}}^{(1)}) d\mathbf{r}. \quad (24)$$

We can now calculate the first-order contribution to the torque $\mathbf{T}^{(1)}$ solely using terms whose definitions we already know, from both the leading-order solution for translation and the solution for a rotating sphere in a Newtonian fluid, which we use to define the term $\mathbf{S}(\mathbf{r})$. The term $\hat{\boldsymbol{\tau}}_p^{(1)} - 2\chi(\omega)\hat{\mathbf{e}}^{(1)}$ in Eq. (24) can be determined simply from Eq. (14) for the case where $n = 2$

$$\begin{aligned} \hat{\boldsymbol{\tau}}_p^{(1)} - 2\chi(\omega)\hat{\mathbf{e}}^{(1)} = -\alpha(\hat{\boldsymbol{\tau}}_p^{(0)} * \hat{\boldsymbol{\tau}}_p^{(0)}) + \hat{\mathbf{v}}^{(0)} * \nabla \hat{\boldsymbol{\tau}}_p^{(0)} \\ - (\nabla \hat{\mathbf{v}}^{(0)T} * \hat{\boldsymbol{\tau}}_p^{(0)} + \hat{\boldsymbol{\tau}}_p^{(0)} * \nabla \hat{\mathbf{v}}^{(0)}). \end{aligned} \quad (25)$$

Using the definition of torque in Eq. (24) and the correspondence relationships as defined in Eq. (18), we arrive at the following equation for the additional contribution to the torque at $\mathcal{O}(\text{Wi})$:

$$\begin{aligned} \mathbf{T}^{(1)} = \chi(\omega)(\hat{V}_1(\omega) * [\chi(\omega)\hat{V}_2(\omega)]) \\ \times \int_V \mathbf{S}(\mathbf{r}) : \left[\alpha(\hat{\boldsymbol{\tau}}_{p,1}^{(0)} \cdot \hat{\boldsymbol{\tau}}_{p,2}^{(0)} + \hat{\mathbf{v}}_1^{(0)} \cdot \nabla \hat{\boldsymbol{\tau}}_{p,2}^{(0)} \right. \\ \left. - \frac{1}{2}(\hat{\mathbf{v}}_1^{(0)T}(\mathbf{r}) \cdot \hat{\boldsymbol{\tau}}_{p,2}^{(0)} + \hat{\boldsymbol{\tau}}_{p,2}^{(0)} \cdot \hat{\mathbf{v}}_1^{(0)}) \right] d\mathbf{r} \\ + \chi(\omega)(\hat{V}_2(\omega) * [\chi(\omega)\hat{V}_1(\omega)]) \\ \times \int_V \mathbf{S}(\mathbf{r}) : \left[\alpha(\hat{\boldsymbol{\tau}}_{p,2}^{(0)} \cdot \hat{\boldsymbol{\tau}}_{p,1}^{(0)} + \hat{\mathbf{v}}_2^{(0)} \cdot \nabla \hat{\boldsymbol{\tau}}_{p,1}^{(0)} \right. \\ \left. - \frac{1}{2}(\hat{\mathbf{v}}_2^{(0)T}(\mathbf{r}) \cdot \hat{\boldsymbol{\tau}}_{p,1}^{(0)} + \hat{\boldsymbol{\tau}}_{p,1}^{(0)} \cdot \hat{\mathbf{v}}_2^{(0)}) \right] d\mathbf{r}. \end{aligned} \quad (26)$$

Upon evaluation of the integrals in Eq. (26) using the symbolic solver Mathematica and the Einstein notation plugin EinS,⁴⁵ we arrive at a simpler expression for the first-order, or $\mathcal{O}(\text{Wi})$, correction to the torque

$$\begin{aligned} \hat{\mathbf{T}}^{(1)} = \frac{27\pi(1-\beta)}{20} \chi(\omega) [(\hat{V}_2(\omega) * [\chi(\omega)\hat{V}_1(\omega)]) \\ - (\hat{V}_1(\omega) * [\chi(\omega)\hat{V}_2(\omega)])] \mathbf{e}_3, \end{aligned}$$

with the torque acting in the \mathbf{e}_3 direction as expected. The particle is torque-free, and thus, the torque generated by the interacting flow fields must be exactly counteracted by the particle's rotation. We can thus solve for the particle rotation by the following balance:

$$\hat{\mathbf{T}}^{(0)} + \text{Wi}\hat{\mathbf{T}}^{(1)} = 0, \quad (27)$$

where the leading-order dimensionless torque $(\mathbf{T}^{(0)}(\omega)/a^2\eta_0 V_c)$ for a sphere in a viscous Newtonian fluid undergoing a rotation at frequency $\hat{\Omega}$ has the well-known form⁴⁴

$$\hat{\mathbf{T}}^{(0)} = 8\pi\eta^*(\omega)\hat{\Omega}(\omega)\mathbf{e}_3. \quad (28)$$

So, we now have defined all terms of the torque balance

$$\begin{aligned} 8\pi\eta^*(\omega)\hat{\Omega}(\omega) = -\text{Wi} \frac{27\pi(1-\beta)}{20} \chi(\omega) [(\hat{V}_2(\omega) * [\chi(\omega)\hat{V}_1(\omega)]) \\ - (\hat{V}_1(\omega) * [\chi(\omega)\hat{V}_2(\omega)])], \end{aligned}$$

meaning that the angular velocity of the particle is

$$\begin{aligned} \hat{\Omega}(\omega) = -\frac{27(1-\beta)\text{Wi}}{160\eta^*(\omega)} \chi(\omega) [(\hat{V}_2(\omega) * [\chi(\omega)\hat{V}_1(\omega)]) \\ - (\hat{V}_1(\omega) * [\chi(\omega)\hat{V}_2(\omega)])]. \end{aligned} \quad (29)$$

This form of the angular velocity $\hat{\Omega}(\omega)$ arising from the first effects of elasticity can now be used to both model particle rotation in arbitrary 2D flows and to predict the force correction arising from interactions between particle translation and rotation.

C. Calculation of force

The leading-order correction to the force can be calculated using a similar procedure as that for calculating the particle rate of rotation.

We begin by constructing a reciprocal theorem argument using the known flow field components and an arbitrary auxiliary flow, $\hat{\mathbf{v}}'$ and pressure \hat{p}' such that $\hat{\mathbf{v}}'(r \rightarrow \infty) = 0$, $\hat{p}'(r \rightarrow \infty) = 0$, and $\hat{\mathbf{v}}'(r = 1) = \mathbf{u}'$. The deviatoric stress in this flow is $\hat{\boldsymbol{\tau}}' = 2\eta^*(\omega)\mathbf{e}'$, where the rate of strain tensor $\mathbf{e}' = \mathbf{u}' \cdot \mathbf{R}(\mathbf{r})$ and the tensor $\mathbf{R}(\mathbf{r})$, defined in Eq. (32), is known from the solution to the leading-order problem. We can once again construct a standard reciprocal theorem argument

$$\int_V \nabla \cdot [(-\hat{p}'\mathbf{I} + 2\beta\hat{\mathbf{e}}^{(1)} + \hat{\boldsymbol{\tau}}_p^{(1)}) \cdot \hat{\mathbf{v}}'] \, d\mathbf{r} = \int_V \nabla \cdot [(-\hat{p}'\mathbf{I} + \hat{\boldsymbol{\tau}}') \cdot \hat{\mathbf{v}}^{(1)}] \, d\mathbf{r}. \tag{30}$$

As with the above calculation of torque by a similar method, there are several intermediate steps involving further simplification, application of the divergence theorem, and some tedious algebra. Eventually, we arrive at a simple expression for the correction to the force

$$\hat{\mathbf{F}}^{(1)}(\omega) = \int_V \mathbf{R}(\mathbf{r}) : (\hat{\boldsymbol{\tau}}_p^{(1)}(\omega) - 2\chi(\omega)\hat{\mathbf{e}}^{(1)}(\mathbf{r}, \omega)) \, d\mathbf{r}, \tag{31}$$

in which we know $\mathbf{R}(\mathbf{r})$ from the leading-order solution, corresponding to Stokes flow of a Newtonian fluid

$$R_{ijk}(\mathbf{r}) = \frac{3}{4r^3} \left(-r_k\delta_{ij} + \frac{1}{r^2} (3r_i r_j r_k + r_i\delta_{jk} + r_j\delta_{ik} + r_k\delta_{ij}) - \frac{5}{r^4} r_i r_j r_k \right), \tag{32}$$

and the term $\hat{\boldsymbol{\tau}}_p^{(1)}(\mathbf{r}, \omega) - 2\chi(\omega)\hat{\mathbf{e}}^{(1)}(\mathbf{r}, \omega)$ is defined entirely in terms of the leading-order solution, as shown in Eq. (25).

We can thus now evaluate the predicted force correction arising from the interaction of translation and rotation. Note that throughout this derivation up to this point, terms here are indicated as being first order, as they come from interactions of two leading-order, or Stokes, flow fields. However, the overall contribution to the force here will be $\mathcal{O}(\text{Wi}^2)$, due to its dependence on the particle rotation, which scales with Wi as shown in Eq. (29). Thus, the contribution to the force in Eq. (33) will be denoted $\hat{\mathbf{F}}^{(2)}$ rather than $\hat{\mathbf{F}}^{(1)}$ going forward.

The final form of this $\mathcal{O}(\text{Wi}^2)$ force term arising from translation-rotation coupling is

$$\begin{aligned} \hat{\mathbf{F}}^{(2)} = & \chi(\omega) \left(\hat{\boldsymbol{\Omega}}(\omega) * [\hat{V}_1(\omega)\chi(\omega)] \right) \int_V \mathbf{R}(\mathbf{r}) : \left[\alpha \left(\tilde{\boldsymbol{\tau}}_{p,2}^{(0)} \cdot \tilde{\boldsymbol{\tau}}_{p,1}^{(0)} \right) + \tilde{\mathbf{v}}_3^{(0)} \cdot \nabla \tilde{\boldsymbol{\tau}}_{p,1}^{(0)} - \frac{1}{2} \left(\tilde{\mathbf{v}}_3^{(0)T} \cdot \tilde{\boldsymbol{\tau}}_{p,1}^{(0)} + \tilde{\boldsymbol{\tau}}_{p,1}^{(0)} \cdot \tilde{\mathbf{v}}_3^{(0)} \right) \right] \, d\mathbf{r} \\ & + \chi(\omega) \left(\hat{V}_1(\omega) * [\hat{\boldsymbol{\Omega}}(\omega)\chi(\omega)] \right) \int_V \mathbf{R}(\mathbf{r}) : \left[\alpha \left(\tilde{\boldsymbol{\tau}}_{p,1}^{(0)} \cdot \tilde{\boldsymbol{\tau}}_{p,3}^{(0)} \right) + \tilde{\mathbf{v}}_1^{(0)} \cdot \nabla \tilde{\boldsymbol{\tau}}_{p,3}^{(0)} - \frac{1}{2} \left(\tilde{\mathbf{v}}_1^{(0)T} \cdot \tilde{\boldsymbol{\tau}}_{p,3}^{(0)} + \tilde{\boldsymbol{\tau}}_{p,3}^{(0)} \cdot \tilde{\mathbf{v}}_1^{(0)} \right) \right] \, d\mathbf{r} \\ & + \chi(\omega) \left(\hat{\boldsymbol{\Omega}}(\omega) * [\hat{V}_2(\omega)\chi(\omega)] \right) \int_V \mathbf{R}(\mathbf{r}) : \left[\alpha \left(\tilde{\boldsymbol{\tau}}_{p,2}^{(0)} \cdot \tilde{\boldsymbol{\tau}}_{p,2}^{(0)} \right) + \tilde{\mathbf{v}}_3^{(0)} \cdot \nabla \tilde{\boldsymbol{\tau}}_{p,2}^{(0)} - \frac{1}{2} \left(\tilde{\mathbf{v}}_3^{(0)T} \cdot \tilde{\boldsymbol{\tau}}_{p,2}^{(0)} + \tilde{\boldsymbol{\tau}}_{p,2}^{(0)} \cdot \tilde{\mathbf{v}}_3^{(0)} \right) \right] \, d\mathbf{r} \\ & + \chi(\omega) \left(\hat{V}_2(\omega) * [\hat{\boldsymbol{\Omega}}(\omega)\chi(\omega)] \right) \int_V \mathbf{R}(\mathbf{r}) : \left[\alpha \left(\tilde{\boldsymbol{\tau}}_{p,2}^{(0)} \cdot \tilde{\boldsymbol{\tau}}_{p,3}^{(0)} \right) + \tilde{\mathbf{v}}_2^{(0)} \cdot \nabla \tilde{\boldsymbol{\tau}}_{p,3}^{(0)} - \frac{1}{2} \left(\tilde{\mathbf{v}}_2^{(0)T} \cdot \tilde{\boldsymbol{\tau}}_{p,3}^{(0)} + \tilde{\boldsymbol{\tau}}_{p,3}^{(0)} \cdot \tilde{\mathbf{v}}_2^{(0)} \right) \right] \, d\mathbf{r}, \end{aligned} \tag{33}$$

which, when the integrals are evaluated, can be expressed in a simpler form

$$\begin{aligned} \hat{\mathbf{F}}^{(2)} = & \frac{27\pi(1-\beta)}{40} \chi(\omega) \left[\left(\hat{V}_2(\omega) * [\chi(\omega)\hat{\boldsymbol{\Omega}}(\omega)] \right) \mathbf{e}_1 \right. \\ & \left. - \left(\hat{V}_1(\omega) * [\chi(\omega)\hat{\boldsymbol{\Omega}}(\omega)] \right) \mathbf{e}_2 \right] + \frac{63\pi(1-\beta)}{40} \chi(\omega) \\ & \times \left[\left(\hat{\boldsymbol{\Omega}}(\omega) * [\chi(\omega)\hat{V}_2(\omega)] \right) \mathbf{e}_1 - \left(\hat{\boldsymbol{\Omega}}(\omega) * [\chi(\omega)\hat{V}_1(\omega)] \right) \mathbf{e}_2 \right]. \end{aligned} \tag{34}$$

For a complete expression for the force correction arising at $\mathcal{O}(\text{Wi}^2)$, terms arising purely from the translational motion in the \mathbf{e}_1 and \mathbf{e}_2 directions must also be considered. These terms have been derived previously for the Johnson-Segalman and Giesekus models,³¹ and are replicated for the Giesekus model in Appendix A [see Eq. (A1)]. These purely translational components will be included in the total force corrections for all of the example flows in Sec. IV.

IV. EXAMPLE FLOWS

To demonstrate how the general solutions derived in this work can be used to better understand some specific particle trajectories, we

provide three examples: predicting the angular velocity and total force exerted on a particle moving in a circular trajectory, as shown in Fig. 1(a) and described in Fig. 2; predicting the variations in the angular velocity and total force exerted on a particle moving in a sinusoidal trajectory, as shown in Fig. 1(b); and predicting the trajectory of a particle subjected to an external time-varying force in a user-controlled elliptical pattern.

A. Circular trajectory

A particle of radius a moving in a circular trajectory with radius R at a frequency $2\pi f$, as seen in Fig. 1, has a path described as

$$x_1(t) = R \cos(2\pi ft), \quad x_2(t) = R \sin(2\pi ft), \tag{35}$$

which results in a time-varying velocity

$$V_1(t) = -2\pi f R \sin(2\pi ft), \quad V_2(t) = 2\pi f R \cos(2\pi ft). \tag{36}$$

The expressions derived for the angular velocity and the force involve the frequency-space definitions for the imposed velocities, which in this case are

$$\begin{aligned} \hat{V}_1(\omega) &= i2\pi^2 fR(\delta(2\pi f - \omega) - \delta(2\pi f + \omega)) \\ \hat{V}_2(\omega) &= 2\pi^2 fR(\delta(2\pi f - \omega) + \delta(2\pi f + \omega)). \end{aligned} \tag{37}$$

Note that $2\pi f$, rather than the more conventional ω , is used here to denote the frequency of the particle’s traversal of the circular trajectory to avoid confusion as ω has been used throughout this work to denote the frequency variable in the Fourier-space terms. In this case, the characteristic velocity V_c on which terms will be made dimensionless is $V_c = 2\pi fR$. Assuming that the viscoelastic fluid has a single relaxation time λ , we thus define the Deborah number for this unsteady flow to be $De = 2\pi f\lambda$. Using the imposed velocity of the particle defined in Eq. (37), we can calculate the force exerted on this particle at leading order, the particle’s angular velocity and the total correction to the force arising at second order in the Weissenberg number [i.e., at $\mathcal{O}(Wi^2)$], $Wi = De(R/a)$.

First and most straightforwardly, we can calculate the time-dependent force on this particle at leading order using Eq. (20). While Eq. (2) is the expression for the force in frequency space, this can easily be converted to the time domain by taking its inverse Fourier transform $\mathcal{F}^{-1}[\hat{\mathbf{F}}^{(0)}(\omega)] = \mathbf{F}^{(0)}(t)$. The result is then

$$\begin{aligned} \mathbf{F}^{(0)}(t) &= -6\pi \left(\beta \sin(2\pi ft) \right. \\ &\quad \left. + (1 - \beta) \frac{\sin(2\pi ft) - De \cos(2\pi ft)}{1 + De^2} \right) \mathbf{e}_1 \\ &\quad + 6\pi \left(\beta \cos(2\pi ft) + (1 - \beta) \frac{\cos(2\pi ft) + De \sin(2\pi ft)}{1 + De^2} \right) \mathbf{e}_2. \end{aligned} \tag{38}$$

The angular velocity of the particle can be calculated using Eq. (29). Once again, Eq. (29) describes a frequency-space quantity, which can be converted to the time domain with an inverse Fourier transform $\mathcal{F}^{-1}[\hat{\Omega}(\omega)] = \Omega(t)$.

In this case, the angular velocity is found to be a constant, as would be expected for a circular trajectory

$$\begin{aligned} \Omega &= \frac{-27Wi(1 - \beta)}{160} \frac{De}{(1 + De^2)} \mathbf{e}_3, \\ &= \frac{-27(1 - \beta)}{160} \left(\frac{R}{a} \right) \left(\frac{De^2}{1 + De^2} \right) \mathbf{e}_3. \end{aligned} \tag{39}$$

The angular velocity, in this case, is influenced by the Deborah and Weissenberg numbers, as well as the dimensionless polymeric contribution to the viscosity $(1 - \beta)$. Substitution of the definition of the Weissenberg number in this case, $Wi = (R/a)De$, results in an expression for the angular velocity dependent on the viscosity, inverse radius ratio R/a , and Deborah number. We will primarily examine this problem in the context of these dimensionless groups.

Finally, the expression for the second-order, or $\mathcal{O}(Wi^2)$, correction to the time-dependent force—derived using an inverse Fourier transform of its frequency-dependent definition Eq. (34)—arising from coupling between particle rotation and translation is

$$\begin{aligned} \mathbf{F}^{(2)}(t) &= \frac{243\pi}{6400} \left(\frac{R}{a} \right)^2 \frac{De^2(1 - \beta)^2}{(De^2 + 1)^3} \\ &\quad \times \left((3De^3 + 17De)\sin(2\pi ft) + (10 - 4De^2)\cos(2\pi ft) \right) \mathbf{e}_1 \\ &\quad - \left((3De^3 + 17De)\cos(2\pi ft) - (10 - 4De^2)\sin(2\pi ft) \right) \mathbf{e}_2. \end{aligned} \tag{40}$$

The full expression for the force correction arising from purely translational components is too long and unwieldy to print here, but can be provided upon request to the authors via email. However, we can examine its relative influence on the overall force when compared to the force correction arising from rotation–translation coupling. Figure 3 shows the maximum contribution of rotation–translation coupling components of the force and purely translational components. We show the maximum contributions here because, due to the dynamic nature of the solution, the value of each of these corrections varies significantly over time; the maximum gives a clear picture of the magnitude of the force correction throughout the duration of particle motion. From this figure, it is clear that both corrections are highly dependent on the radius ratio a/R . When a/R is very small, the radius of the particle trajectory is much greater than the radius of the particle itself and the trajectory is well-approximated by pure translation. In this limit, the translational component of the force correction dominates. However, as a/R increases, the approximation as pure translation is no longer valid, and the component of the force correction arising from coupling of rotation- and translation-dependent terms becomes increasingly important. It eventually surpasses the purely translational component and thus also must be considered to achieve an accurate understanding of this particle motion. Note that at higher values of the radius ratio a/R , it appears in Fig. 3 that the translation–rotation component of the force correction exceeds the total force correction, which is counter-intuitive. However, this is simply because the values shown here are the maximum absolute value of time-dependent functions. Thus, this would indicate at the points in time where the magnitude of the translation–rotation component of the force exceeds the total value of the force correction, it is being counteracted by the translational component of the force correction.

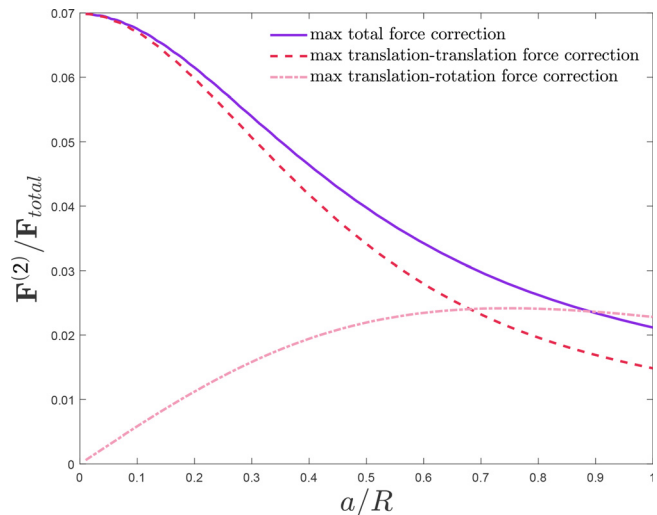


FIG. 3. Maximum total correction to the force arising at second order in Weissenberg number for a Giesekus fluid with $\alpha = 0.3$ and $\beta = 0.001$ is shown as a function of the radius ratio a/R for a constant $Wi = 1$. This shows that the predominant contribution at low a/R comes from translation–translation coupling, and that at high a/R , there is a transition to predominant contributions from rotation–translation coupling.

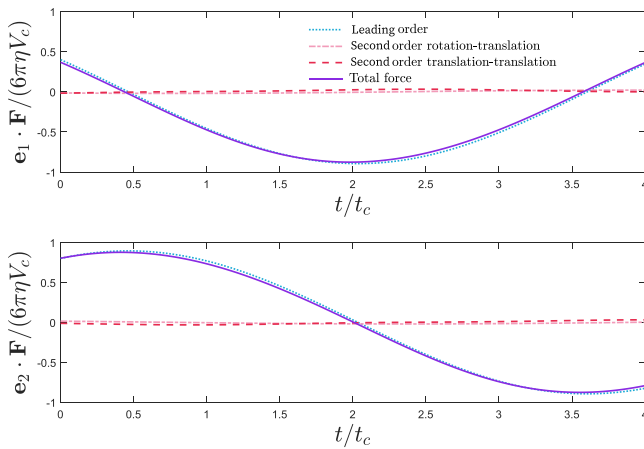


FIG. 4. Variation in the total force over time for a particle moving in a circular trajectory with $De = 0.5$, inverse radius ratio $R/a = 2$, $\beta = 0.001$, and $\alpha = 0.3$ is shown, as well as individual components of that force arising at leading order ($\mathcal{O}(1)$) in addition to the second-order ($\mathcal{O}(Wi^2)$) corrections from both translation-translation and translation-rotation coupling.

We can also examine the time-dependent force exerted on a particle undergoing a specific circular trajectory in a Giesekus fluid. In this case, we examine a fluid with a moderate mobility parameter of $\alpha = 0.3$ and $\beta = 0.001$, indicating $\eta_p \gg \eta_s$, as is often the case for semidilute or entangled polymer solutions.^{23,46} We can examine a specific radius ratio $a/R = 0.5$ and a Deborah number $De = 0.5$, meaning the Weissenberg number is $Wi = 1$, which approaches the upper limit at which this solution is expected to be valid. Figures 4 and 5 show the dynamic variations in the total force exerted on the particle in the e_1 and e_2 directions for a short segment of dimensionless time t/t_c . Once again, we can see that for this case the magnitude of the force corrections arising from rotation-translation coupling and pure translation are of roughly equal magnitude, and overall contribute to a

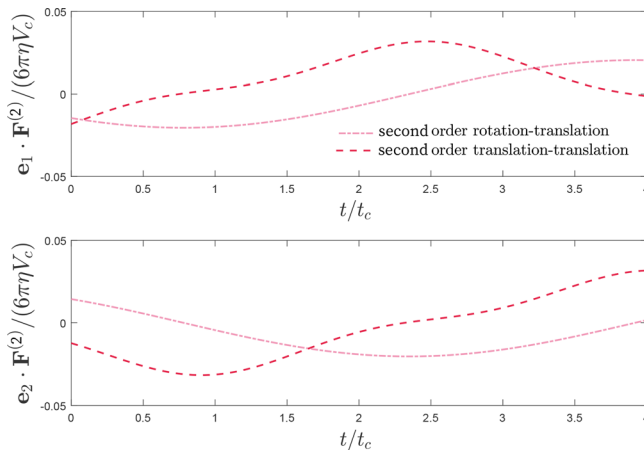


FIG. 5. The second-order contributions to the force are shown here for a Deborah number $De = 0.5$, inverse radius ratio $R/a = 2$, $\beta = 0.001$, and $\alpha = 0.3$, indicating that the corrections arising from translation-translation and translation-rotation coupling are on the same order of magnitude.

small but noticeable decrease in the magnitude of the total force when compared to the leading-order solution on its own; for this specific and relatively moderate set of parameters, the total decrease in the force is, on average, about 4%.

While investigating specific flows in a fluid with known parameters can be illuminating, we also have, as shown in Fig. 2, a broad operating space in which these parameters can be varied. In order to best understand how those parameters affect the total force being exerted on the particle, we can examine contour plots of the maximum total correction to the force at second order in Wi , or $\mathcal{O}(Wi^2)$, as a function of the Deborah number De , the inverse radius ratio R/a , and the Giesekus mobility parameter α . Figure 6 shows how these contours vary for a fixed value of mobility parameter $\alpha = 0.3$, with De varying from 0 to 0.5 and the inverse radius ratio R/a varying from 0 to 2, or from the case in which we can approximate the motion as pure rotation to that of a particle moving in a trajectory with a radius twice that of its own. Because the Weissenberg number is $Wi = (R/a)De$ and the force correction is directly dependent on Wi , we would intuitively expect the greatest magnitude of the force correction to occur in the top-right area of the plot, which represents the highest values of Wi . However, we can also see from this plot that increasing the inverse radius ratio (R/a) at a constant De and increasing De at a constant inverse radius ratio have slightly different impacts on the magnitude of the force correction, with increase in the inverse radius ratio resulting in a more rapid increase in overall force correction than with an increase in De .

In Fig. 7, we vary the mobility parameter α between $\alpha = 0$, or the Oldroyd-B model, and $\alpha = 0.5$ —commonly recognized to be the physically realistic limit of the Giesekus model¹⁸—and the Deborah number from 0 to 1 for a constant Weissenberg number of $Wi = 1$. The constant Wi is maintained by adjusting the inverse radius ratio to compensate for changes in Deborah number, to satisfy the constraint $Wi \equiv De(R/a)$. Here we can see that at any value of the Deborah

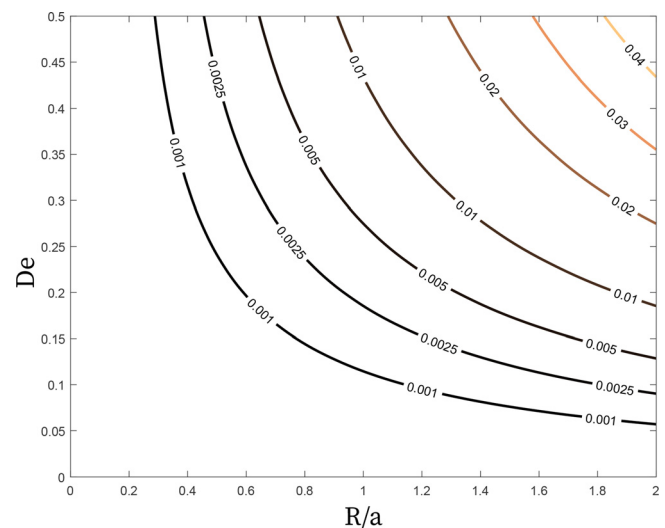


FIG. 6. Contours of the maximum total correction to the force arising at second order in Wi for a Giesekus fluid with $\alpha = 0.3$ and $\beta = 0.001$ is shown as a function of the Deborah number De and inverse radius ratio R/a . The Weissenberg number $Wi = De(R/a)$ increases toward the upper right corner.

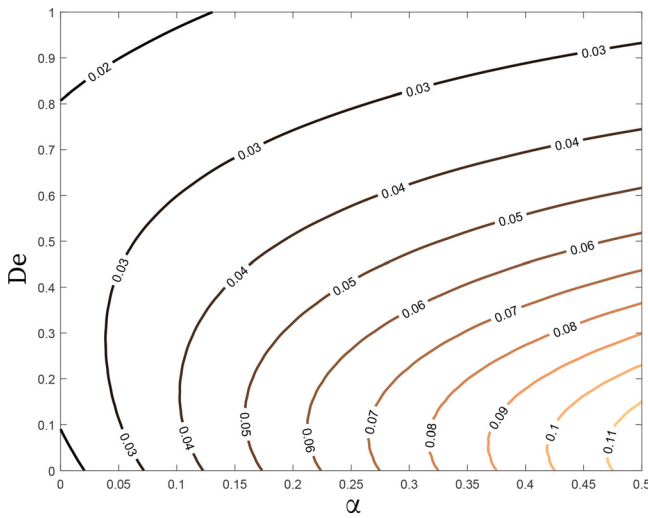


FIG. 7. Contours of the maximum total correction to the force arising at second order in Wi for a Giesekus fluid with $\beta = 0.001$ are shown as a function of the Deborah number and mobility parameter α for a constant value of $Wi = 1$, indicating that the inverse radius ratio R/a is adjusted as needed for changing De to maintain a constant Weissenberg number via the relationship $Wi/De = R/a$.

number, increasing the mobility number, or increasing the extent of shear thinning, increases the predicted magnitude of the force correction and thus enhances the total effect of nonlinear viscoelasticity in the system. We see the opposite trend in this case for unsteady effects, where at a given value of α , the total magnitude of the force correction tends to decrease with increasing Deborah number above $De = 0.1$. This can be attributed to the adjustment of R/a to maintain the Weissenberg number $Wi = 1$; as seen in Fig. 3, the total magnitude of the force correction is higher at larger values of R/a due to the larger contributions from the purely translational terms.

We can perform a similar analysis for a system in which, again, the mobility parameter α and the Deborah number both range from 0 to 0.5, but rather than Weissenberg number being held constant the inverse radius ratio is held constant at $R/a = 2$ (meaning the radius of the particle trajectory is twice the radius of the particle itself), so that $Wi = 2De$. Contours of the maximum total correction to the force for such a system are shown in Fig. 8. In this case, once again, the increase in Wi with increasing De would be intuitively expected to increase the magnitude of the force correction regardless of other factors. However, we can also see that at a given De (and thus given Wi), increasing the mobility parameter again enhances the effects of elasticity in the system, and that this effect is more drastic at lower values of the mobility parameter α .

Finally, it can be useful to examine our solution in various limits, to ensure we recover the expected behavior in those limits and to better understand how this solution relates to other, previously known ones. For example, in the limit of $R/a \rightarrow \infty$ and $De \rightarrow 0$, we would expect to recover the solution of steady 1D motion of a spherical particle through a viscoelastic fluid. Indeed, in this limit, the angular velocity $\Omega \rightarrow 0$, indicating that the particle does not rotate, and the second-order force correction arising from rotation-translation coupling subsequently goes to 0 as well. Only the purely translational term remains,

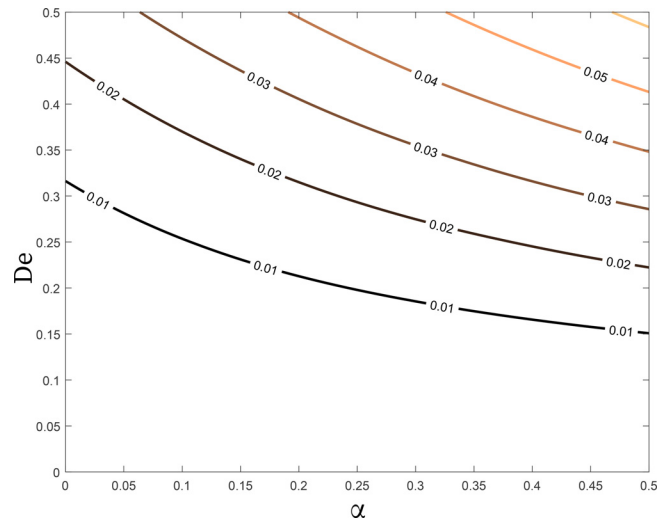


FIG. 8. Maximum total correction to the force arising at second order in Wi for a Giesekus fluid with $\beta = 0.001$ is shown as a function of the Deborah number De and mobility parameter α for a constant inverse radius ratio $R/a = 2$, resulting in a variable Weissenberg number $Wi = De(R/a) = 2De$.

as would be expected for this case, and this purely translational term has been shown to be in agreement with previously derived solutions in relevant limits.^{6,31} Additionally, for the case of $\beta \rightarrow 1$, we would expect to recover the Stokes solution for a Newtonian fluid, which we do, as all nonlinear terms scale directly with $1 - \beta$ and thus go to zero, and the terms at leading order arising from the polymeric stress scale with $1 - \beta$ as well and also go to zero. The solution thus behaves the way we would expect in these limits, providing some indication that we are accurately capturing the flow behavior.

B. Sinusoidal trajectory

Due to the generality of the solution derived in Sec. III, we can use the same exact steps used in Sec. IV A to analyze a totally different particle trajectory. We will now look at a particle moving in a sinusoidal trajectory as shown in Fig. 1(b), which has a time-dependent position

$$r_1(t) = V_0 t, \quad r_2(t) = Y_0 \sin(2\pi f t), \quad (41)$$

which results in a sinusoidally varying velocity

$$v_1(t) = V_0, \quad v_2(t) = 2\pi f Y_0 \cos(2\pi f t), \quad (42)$$

which, in frequency space, has the form

$$\hat{v}_1(\omega) = V_0 \delta(\omega), \quad \hat{v}_2(\omega) = \pi 2\pi f Y_0 (\delta(2\pi f - \omega) + \delta(2\pi f + \omega)). \quad (43)$$

In this case, the characteristic velocity V_c can once again be defined as $V_c = 2\pi f Y_0$, as described in Sec. II. For simplicity, we will assume throughout this example that the constant velocity in the e_1 direction is given by $V_0 = 2\pi f Y_0$, though that does not necessarily have to be the case. Using $V_0 \neq 2\pi f Y_0$ would simply result in an additional constant scaling factor in some terms. The Weissenberg and

Deborah numbers in this case, following the formulation of Sec. II, will be $De = 2\pi f\lambda$ and $Wi = 2\pi f\lambda Y_0/a = De(Y_0/a)$, with the term Y_0/a serving a similar function as the inverse radius ratio R/a in the case of a circular trajectory.

As was the case for the circular trajectory, we can use this imposed velocity to calculate the leading-order force exerted on the particle, the angular velocity, and the second-order correction to the force arising from both pure translation and translation-rotation coupling.

The dimensionless force at leading order in Wi , or the Stokes flow limit, exerted on a particle undergoing this trajectory is

$$\mathbf{F}(t) = 6\pi\mathbf{e}_1 + 6\pi\left(\beta \cos(2\pi ft) + (1 - \beta) \frac{\cos(2\pi ft) + De \sin(2\pi ft)}{1 + De^2}\right)\mathbf{e}_2, \quad (44)$$

which, in the limit of $De \rightarrow 0$, recovers the Stokes flow solution, and in the limit of $\beta \rightarrow 1$ recovers the behavior of a Newtonian fluid.

In this case, the angular velocity of the particle is time-dependent and takes the form

$$\Omega(t) = \frac{-27(1 - \beta)Wi}{160} \times \frac{De((1 + \beta)De \cos(2\pi ft) + (De^2\beta - 1) \sin(2\pi ft))}{(1 + De^2)(1 + De^2\beta^2)}, \quad (45)$$

or, when the Weissenberg number is eliminated in favor of the Deborah number and the geometric ratio Y_0/a

$$\Omega(t) = \frac{-27(1 - \beta)}{160} \left(\frac{Y_0}{a}\right) \times \frac{De^2((1 + \beta)De \cos(2\pi ft) + (De^2\beta - 1) \sin(2\pi ft))}{(1 + De^2)(1 + De^2\beta^2)}. \quad (46)$$

We can visualize the particle rotation over the course of the particle's trajectory, as shown in Fig. 9. The top panel of this figure shows the particle trajectory over time, while the bottom panel tracks the angular velocity over that same time period. Lining the bottom of this figure is a series of particle "snapshots" over the time frame considered, with the black line providing a fixed reference for the particle's rotational position. It is clear from both the y-axis scale of the bottom panel and the particle snapshots at the bottom of this figure that the actual angular velocity and resultant displacement of the particle arising from its changing rotation is rather small, especially since the direction of rotation changes back and forth throughout the cyclical movement, resulting in an average net rotational displacement of zero. However, even though the rotation only results in these small, cyclic displacements, it does significantly impact the total correction to the force. The force correction arising from the rotation-translation coupling at second order ($\mathcal{O}(Wi^2)$) is

$$\begin{aligned} F_1 &= \frac{-243\pi(1 - \beta)^2 De (De(10\beta + 3)(4De^4 + 5De^2 + 1) + ((5\beta - 6)De^4 - (37\beta + 38)De^2 + 10) \sin(4\pi ft))}{12800(De^2 + 1)^2(4De^2 + 1)(\beta^2 De^2 + 1)} \\ &\quad - \frac{243\pi(1 - \beta)^2 De (5De^2 + 2\beta(3De^4 + 19De^2 - 5) - 37) \cos(4\pi ft)}{12800(De^2 + 1)^2(4De^2 + 1)(\beta^2 De^2 + 1)}, \quad (47) \\ F_2 &= \frac{243\pi(1 - \beta)^2 De (De(\beta(De^2 - 1) - 2) \cos(2\pi ft) - ((2\beta + 1)De^2 - 1) \sin(2\pi ft))}{640(De^2 + 1)^2(\beta^2 De^2 + 1)}. \end{aligned}$$

Once again, the expression for the force correction arising from purely translational term is very long and not included here for convenience, but will be made available upon request to the authors via email. However, we can use similar techniques as in Sec. IV A to visualize the contributions to the force at second order, by using a series of contour plots to examine how different variables affect the total force.

Figure 10 shows the contours of the maximum value of leading-order correction of the force as a function of De and the Giesekus mobility parameter α . The top row of the figure shows this correction for a constant Weissenberg number $Wi = 1$, and the bottom row for a variable $Wi = 2De$, with the \mathbf{e}_1 component of the force on the left and the \mathbf{e}_2 component on the right in each case.

In both cases, similar trends can be observed as in the case of a circular trajectory. For example, increasing the mobility parameter at any given De again increases the impact of elasticity and shear-thinning and results in a greater correction to the overall force. Similar

trends also emerge as were observed in the circular case for the dependence on De in the case of constant $Wi = 1$, which in this case indicates that increasing De must be compensated for by decreasing the ratio of the trajectory amplitude to particle radius Y_0/a . Increasing De in the constant Weissenberg number ($Wi = 1$) case tends, in fact, to reduce the total force correction at a given mobility parameter. This effect is observed only in the \mathbf{e}_2 direction, and interestingly only at mobility parameters $\alpha > 0.1$, below which increasing De at constant Wi causes an increase in the total force correction. For the case of a variable Weissenberg number of $Wi = 2De$, or the bottom row in Fig. 10, we again observe that, as would be intuitively expected, the maximum force correction increases with De , since that corresponds directly to an increase in the Weissenberg number. We can also see that the impact of this increase in Deborah number is more drastic at lower values of the Giesekus mobility parameter, for both the \mathbf{e}_1 and \mathbf{e}_2 directions.

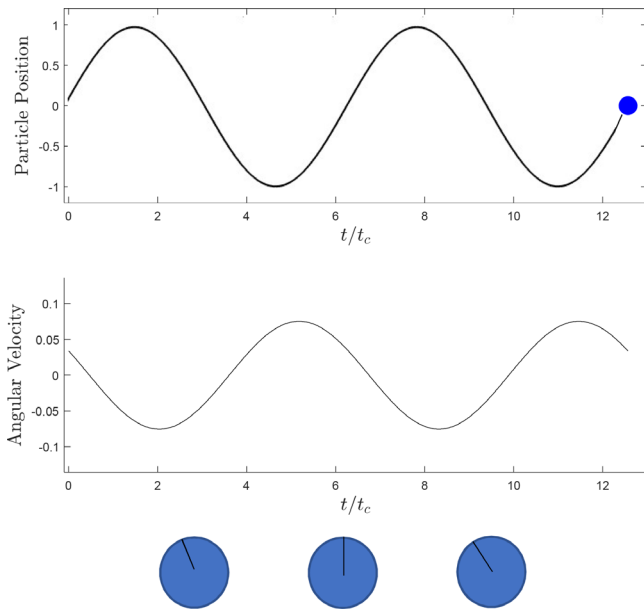


FIG. 9. Angular velocity over time for a particle executing a sinusoidal trajectory, with particle position shown in the upper panel of the figure and the angular velocity in the lower panel. The circles at the bottom of the figure are snapshots of the particle’s rotational position over time, with the black line providing a reference. For animated gif version of this figure, see: <http://tinyurl.com/3h32286y>.

C. Particle trajectory in response to an externally applied time-dependent force

Here, we describe a particle trajectory in which a force is being applied to the particle through some external field, as in cases of optically or magnetically controlled particle movement.^{32,37} In such cases, the force–velocity relationship described in Eqs. (33) and (A1) can be inverted and used to predict how the particle will move under the influence of a controlled external force. The method for inverting this relationship has been previously described^{31,47} and is summarized in Appendix B.

In this case, we will examine a forcing protocol described as

$$F_1(t) = M \cos(2\pi ft), \quad F_2(t) = M \sin(2\pi ft + \psi), \quad (48)$$

or, in frequency space

$$\hat{F}_1(\omega) = M\pi(\delta(2\pi f - \omega) + \delta(2\pi f + \omega)), \quad (49)$$

$$\hat{F}_2(\omega) = -i\pi M(e^{i\psi}\delta(2\pi f - \omega) - e^{-i\psi}\delta(2\pi f + \omega)), \quad (50)$$

in which M indicates the magnitude of the force, $2\pi f$ indicates frequency, and ψ represents a phase shift between the \mathbf{e}_1 and \mathbf{e}_2 components of the imposed force such that for $\psi = 0$ a circular trajectory may be expected, and at $\psi = \pi/2$, we return to a simple, time-dependent 1D translation.

In this case, since it is a force being imposed, not a velocity, it is useful to briefly reconsider the definition of the Weissenberg number in this context. Since it depends on the particle’s velocity, which should scale as $V_c = 2\pi fR = M/a\eta_0$, the Weissenberg number is defined as $Wi = M\lambda/\eta_0 a^2$. As the characteristic timescale t_c in this case is again

$t_c = 1/(2\pi f)$, the definition of the Deborah number remains $2\pi f\lambda$, as it was in previous examples.

In this case, the primary quantity of interest is the expected trajectory of the particle. While the inverted force–velocity relationship obviously produces a velocity, the trajectory can be determined by integrating that velocity from 0 to an arbitrary time t . Following that protocol, we can calculate the displacement at leading order in Wi , or $\mathcal{O}(1)$:

$$x_1(t) = \frac{(1 - \beta)De \cos(2\pi ft) + (1 + De^2)\beta \sin(2\pi ft)}{De(1 + De^2\beta^2)}, \quad (51)$$

$$x_2(t) = -\frac{2 \sin(\pi ft)}{De(1 + (De\beta)^2)}((1 - \beta)De \cos(\pi ft - \psi) + (1 + De^2\beta) \sin(\pi ft - \psi)).$$

As is the case for the velocity-driven circular trajectory described in Sec. IV A, the rotation of the particle is a constant and has a very similar form to Eq. (39)

$$\Omega = \frac{-27Wi(1 - \beta) De \cos(\psi)}{160(1 + De^2)} \mathbf{e}_3, \quad (52)$$

which when $\psi = 0$ reduces to the predicted rotation for a circular trajectory, as would be expected; at $\psi = \pi/2$, no rotation is predicted, which is also consistent with unidirectional translation.

The second-order, or $\mathcal{O}(Wi^2)$, contributions to the total expression for displacement are once again too lengthy to be printed, but we can visualize the predicted particle displacement. Figures 11–13 show the predicted displacement for particles under the influence of an external force described above for a variety of parameter values.

In Fig. 11, we show the predicted trajectory for a particle starting at $(1, -1)$, moving through a fluid with a Giesekus mobility parameter of $\alpha = 0.3$, a Deborah number of $De = 0.5$, and a Weissenberg number of $Wi = 1$. The trajectory is shown for a variety of values of ψ , corresponding to increasingly elliptical trajectories as ψ increases. Such trajectories have been experimentally considered by Spatafora-Salazar and coworkers.³⁶ We see, as we would expect, a circular trajectory for $\psi = 0$, a straight line for $\psi = \pi/2$, and ellipses of various aspect ratios for intermediate values of ψ . As a result of the particle’s starting location and the introduced “lag” between the imposed force and immediately resulting displacement, all of these trajectories intersect at the starting point $(1, -1)$, but this intersection is not necessarily at a vertex of the elliptical trajectory.

We can also examine the case of varying De (i.e., the oscillatory frequency) with a constant phase shift ψ , as shown in Fig. 12. This figure shows the predicted trajectory for a particle subjected to this forcing protocol with $\psi = 0$ and $Wi = 1$ in a fluid with parameters $\beta = 0.001$ and $\alpha = 0.3$. One can see clearly in this figure that increasing the Deborah number decreases the predicted radius of the particle’s trajectory if we keep the Weissenberg number fixed, recovering the behavior predicted in the velocity-controlled flows examined in previous examples, which indicated that for a constant Wi , any increase in De must have an attendant decrease in R/a . Additionally, we can see in this figure that the predicted total radius of the particle’s trajectory is larger for the cases in which correction terms have been included than for the leading-order solution, which is also consistent with our observations in Sec. IV A. In that case, we saw that the inclusion of the second-order correction terms decreased the total magnitude

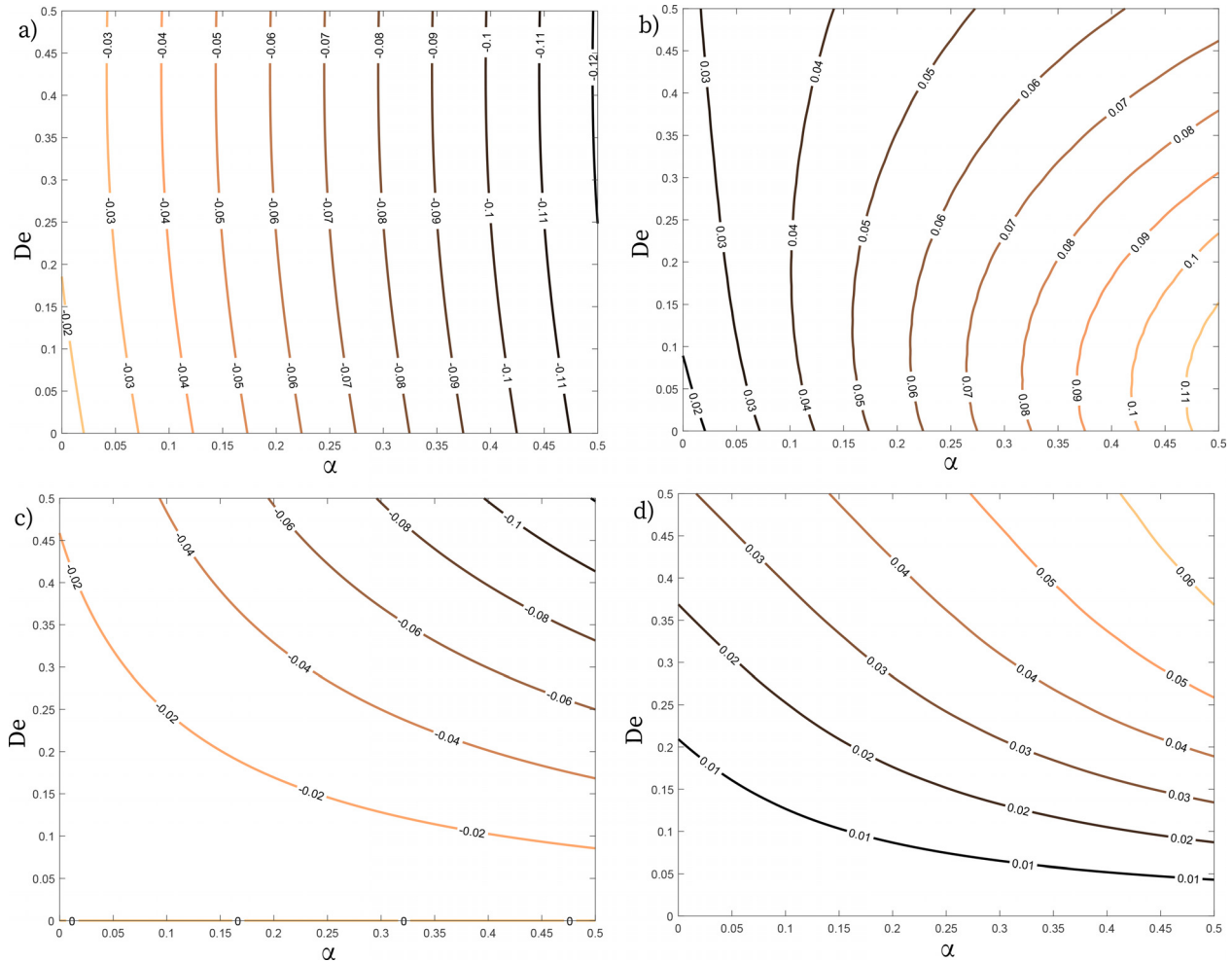


FIG. 10. (a) Contours of the maximum total correction to the force in the e_1 direction for a constant $Wi = 1$ as De and α are varied; (b) contours of the maximum total correction to the force in the e_2 direction for a constant $Wi = 1$; (c) contours of the maximum total correction to the force in the e_1 direction for a constant $Wi = 2De$; and (d) contours of the maximum total correction to the force in the e_2 direction for a constant $Wi = 2De$.

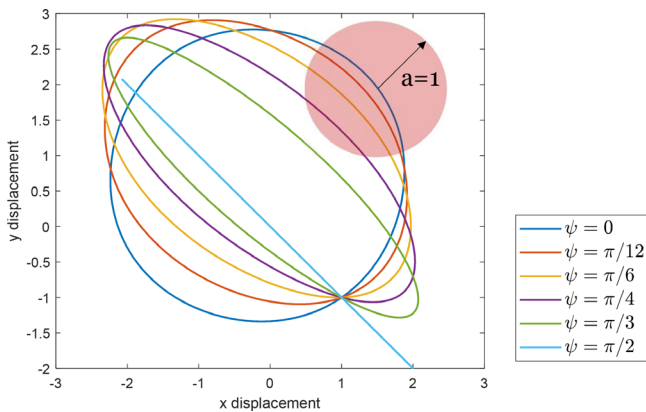


FIG. 11. The predicted trajectory of a particle subjected to the described time-dependent forcing protocol for a variety of ψ values, with $De = 0.5$, $\beta = 0.001$, and $\alpha = 0.3$.

of the expected force exerted on a particle executing a specific trajectory; it follows logically that for the case of a known force being exerted on the particle, the result will be a greater overall displacement.

Though its impact is shown clearly in Fig. 12, inclusion of the second-order terms cause the trajectory to differ from the significantly simpler leading-order predictions in even more dramatic ways for phase shifts of $\psi \neq 0$. Figure 13 shows the trajectory including only the leading-order terms as well as the trajectory involving second-order corrections for a relatively small phase shift of $\psi = \pi/12$ and moderate Deborah number of $De = 0.5$ for a particle immersed in a fluid with $\alpha = 0.3$ and $\beta = 0.001$. The small phase shift if $\psi = \pi/12$ results in a nearly circular elliptical trajectory with a low aspect ratio. While the total radius of the predicted trajectory is slightly (though noticeably) larger for the full solution including the second-order correction terms, it is clearly offset from the leading-order solution at an angle. This indicates that incorporating the second-order corrections calculated in this work is key for accurate prediction of a particle's

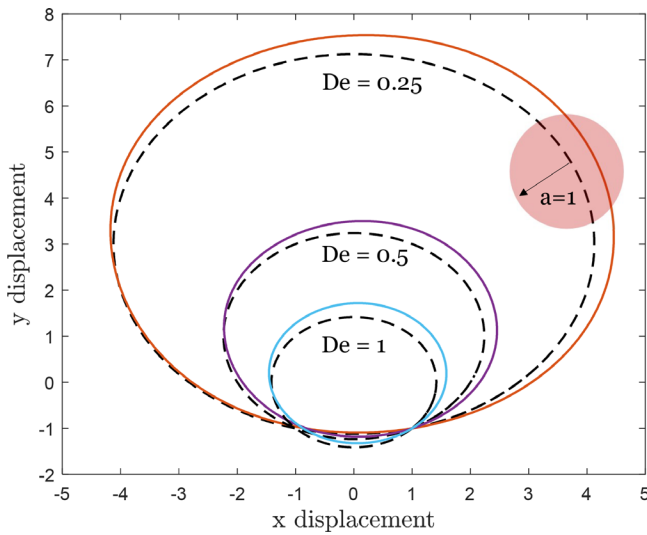


FIG. 12. The predicted trajectory of a particle subjected to the described time-dependent forcing protocol with $\psi = 0$, in a Giesekus fluid with $\beta = 0.001$, and $\alpha = 0.3$ for a variety of Deborah numbers as indicated on the figure. The dashed black lines indicate the leading-order solution and solid, colored lines indicate the total, corrected solution including second-order terms.

trajectory when subjected to a given forcing protocol, as not only will the radius of the particle’s trajectory be larger than the simple leading-order approximation would indicate, but the trajectory will likely also be offset or rotated from the leading-order Stokes-flow approximation.

V. DISCUSSION

In this work, we have demonstrated a method for decomposing and systematically analyzing the time-dependent 2D translation of a

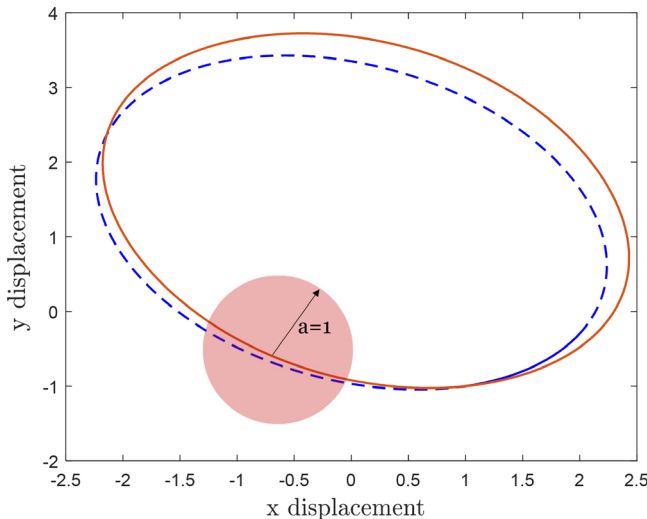


FIG. 13. The predicted trajectory of a particle subjected to the described time-dependent forcing protocol given by Eq. (48) with $\psi = \pi/12$, at $De = 0.5$ in a Giesekus fluid with $\beta = 0.001$, and $\alpha = 0.3$. The dashed blue line indicates the leading-order solution, and the solid red line indicates the total, corrected solution including second-order terms.

small spherical particle moving through a viscoelastic fluid described by the Giesekus model. An asymptotic expansion of the governing equations in terms of the Weissenberg number was described, which is valid in the limit of low Weissenberg number or weak elasticity. The known leading-order, or Stokes-flow, solutions are related to the frequency-space variables using correspondence relationships. Using the Lorentz reciprocal theorem, the angular velocity Ω of the particle arising from interactions of the leading-order velocity fields and correction to the force arising at $\mathcal{O}(Wi^2)$ from coupling of particle rotation and translation are calculated. The derived solution for the angular velocity and the force correction are very general and can be used, in principle, to describe a variety of different particle trajectories; they are also invertible and can be used to describe particle movement resulting from an imposed force.

We have also shown how this general solution can be used to calculate the angular velocity and total force exerted on a particle executing specific two-dimensional motions, namely, a circular trajectory and a sinusoidal trajectory. Our analysis illustrates that for many 2D particle trajectories, it is crucial to consider the rotation-translation coupling to achieve an accurate analysis of the particle motion. We showed in detail how interplay of the Deborah number, the Weissenberg number, radius ratio, and the Giesekus mobility parameter α affects the predicted correction to the force arising at $\mathcal{O}(Wi^2)$. Additionally, we have shown that this method can be used to predict the trajectory over time for a particle subject to some known forcing protocol and that the particle’s predicted trajectory deviates substantially from the simpler leading-order approximation not only in size but in a positional offset. This indicates that in medical applications, such as micro- or nanorobotics, where high accuracy is needed in steering and predicting the trajectory a particle will take through a viscoelastic fluid when subjected to some external force, it is key to consider these higher-order correction terms.

The directed motion of spherical particles in nanorobotics and other applications often relies on trial-and-error testing for determining how the object of interest will move due to a given force. The solutions derived in this work open up the possibility that, given an appropriate model and some calibration to match fluid properties, the particle’s trajectory can be predicted in response to a given force without the need for extensive trial-and-error. This also highlights the generality of this method; once a model and appropriate parameters are known for a fluid of interest, its response to any arbitrary forcing protocol within the limitations of this work—namely, low Reynolds numbers $Re \ll 1$ and low Weissenberg numbers $Wi \leq 1$ —can be predicted.

ACKNOWLEDGMENTS

M.A.J. was supported in part by funding from Aramco Americas through the MIT Energy Initiative.

AUTHOR DECLARATIONS

Conflict of Interest

The authors have no conflicts to disclose.

Author Contributions

Mary Agnes Joens: Conceptualization (equal); Data curation (equal); Formal analysis (equal); Investigation (equal); Methodology (equal); Writing – original draft (equal); Writing – review & editing (equal).

Patrick S. Doyle: Project administration (supporting); Resources (supporting); Writing – review & editing (supporting). **Gareth H. McKinley:** Project administration (equal); Resources (equal); Writing – review & editing (equal). **James W Swan:** Conceptualization (lead); Methodology (equal); Project administration (equal); Resources (equal).

DATA AVAILABILITY

The data that support the findings of this study are available from the corresponding author upon reasonable request.

APPENDIX A: FORCE CORRECTION FOR PURE TRANSLATION

Throughout this work, the total correction to the force at second order has included the purely translational component of that force in addition to the rotation–translation component. This force contribution was derived in a prior paper about 1D translation in viscoelastic fluids³¹ and is reproduced here. The form of the translation-only portions of the force at second order for a Giesekus fluid with a single relaxation time is

$$\begin{aligned} \hat{\mathbf{F}}_i^{(2)}(\omega) = & \frac{6\pi(1-\alpha)(1-\beta)^2\alpha}{175}\chi(\omega)\left([\hat{V}_i(\omega)\chi(\omega)] * \left[\chi(\omega)\left(\frac{\chi(\omega)[\hat{V}_i(\omega) * \hat{V}_i(\omega)\chi(\omega)]}{\eta(\omega)}\right)\right]\right) \\ & + \frac{5652\pi(1-\beta)^2\alpha^2}{2275}\chi(\omega)([\hat{V}_i(\omega)\chi(\omega)] * [\hat{V}_i(\omega)\chi(\omega) * \hat{V}_i(\omega)\chi(\omega)]) \\ & - \frac{5652\pi(1-\beta)^2\alpha^2}{2275}\chi(\omega)([\hat{V}_i(\omega)\chi(\omega)] * [\chi(\omega)(\hat{V}_i(\omega) * \hat{V}_i(\omega)\chi(\omega))]) \\ & - \frac{3\pi(1-\alpha)(1-\beta)^2}{175}\chi(\omega)\left(\left[\frac{\chi(\omega)(\hat{V}_i(\omega) * [\hat{V}_i(\omega)\chi(\omega)])}{\eta^*(\omega)}\right] * [\hat{V}_i(\omega)\chi(\omega)]\right) \\ & - \frac{2826\pi\alpha(1-\beta)}{2275}\chi(\omega)(\hat{V}_i(\omega) * [\chi(\omega)(\hat{V}_i(\omega)\chi(\omega))] * [\hat{V}_i(\omega)\chi(\omega)]) \\ & - \frac{3\pi(1-\alpha)(1-\beta)^2}{175}\chi(\omega)\left(\hat{V}_i(\omega) * \left[\frac{\chi(\omega)\chi(\omega)[\hat{V}_i(\omega) * \hat{V}_i(\omega)\chi(\omega)]}{\eta^*(\omega)}\right]\right) \\ & - \frac{1548\pi(1-\beta)}{25025}\chi(\omega)(\hat{V}_i(\omega) * [\chi(\omega)[\hat{V}_i(\omega) * \hat{V}_i(\omega)\chi(\omega)]]), \end{aligned} \tag{A1}$$

where *i* indicates the direction of translation. This solution collapses to the solution for an Oldroyd-B fluid for the case $\alpha = 0$.

APPENDIX B: SECOND-ORDER VELOCITY IN TERMS OF AN IMPOSED FORCE

In order to calculate the predicted particle displacement in response to a known external force as discussed in Sec. IV C, it is necessary first to calculate the predicted velocity in response to a

known force by inverting the force–velocity relationships in Eqs. (34) and (A1).

This derivation is simpler when convolution terms, such as those in Eq. (34), are re-expressed as integrals using the following relationship:

$$\hat{f}(\omega) * \hat{g}(\omega) = \frac{1}{2\pi} \int_{-\infty}^{\infty} \int_{-\infty}^{\infty} \hat{f}(\omega_1)\hat{g}(\omega_2)\delta(\omega - \omega_1 - \omega_2)d\omega_1d\omega_2, \tag{B1}$$

such that, for example, Eq. (34) would appear as

$$\begin{aligned} \hat{\mathbf{F}}^{(2)} = & \frac{1}{(2\pi)^2}\mathbf{e}_1 \int \int_{-\infty}^{\infty} K_1(\omega_1, \omega_2, \omega_3)[\hat{V}_2(\omega_1)\hat{V}_2(\omega_2)\hat{V}_1(\omega_3) - \hat{V}_2(\omega_1)\hat{V}_1(\omega_2)\hat{V}_2(\omega_3)]d\omega_1d\omega_2d\omega_3 \\ & - \frac{1}{(2\pi)^2}\mathbf{e}_1 \int \int_{-\infty}^{\infty} K_2(\omega_1, \omega_2, \omega_3)[\hat{V}_2(\omega_1)\hat{V}_1(\omega_2)\hat{V}_2(\omega_3) - \hat{V}_1(\omega_1)\hat{V}_2(\omega_2)\hat{V}_2(\omega_3)]d\omega_1d\omega_2d\omega_3 \\ & + \frac{1}{(2\pi)^2}\mathbf{e}_2 \int \int_{-\infty}^{\infty} K_1(\omega_1, \omega_2, \omega_3)[\hat{V}_1(\omega_1)\hat{V}_2(\omega_2)\hat{V}_1(\omega_3) - \hat{V}_1(\omega_1)\hat{V}_1(\omega_2)\hat{V}_2(\omega_3)]d\omega_1d\omega_2d\omega_3 \\ & - \frac{1}{(2\pi)^2}\mathbf{e}_2 \int \int_{-\infty}^{\infty} K_2(\omega_1, \omega_2, \omega_3)[\hat{V}_2(\omega_1)\hat{V}_1(\omega_2)\hat{V}_1(\omega_3) - \hat{V}_1(\omega_1)\hat{V}_2(\omega_2)\hat{V}_1(\omega_3)]d\omega_1d\omega_2d\omega_3, \end{aligned} \tag{B2}$$

where the transfer functions K_1 and K_2 take the form

$$\begin{aligned}
 K_1(\omega_1, \omega_2, \omega_3) &= \frac{-729(1 - \beta)^2 \pi}{4000\eta^*(\omega_1 + \omega_2 + \omega_3)} \chi(\omega_1 + \omega_2 + \omega_3) \\
 &\quad \times \chi(\omega_2 + \omega_3)\chi(\omega_2 + \omega_3)\chi(\omega_3), \\
 K_2(\omega_1, \omega_2, \omega_3) &= \frac{-1701(1 - \beta)^2 \pi}{4000\eta^*(\omega_1 + \omega_2 + \omega_3)} \chi(\omega_1 + \omega_2 + \omega_3) \\
 &\quad \times \chi(\omega_1 + \omega_2)\chi(\omega_2)\chi(\omega_3).
 \end{aligned}
 \tag{B3}$$

Relationships of this type are used extensively in our previous work studying 1D translation.³¹ For the purpose of the following derivation, we will adopt the general notation used there, with transfer functions $\zeta_1(\omega)$ and $\zeta_3(\omega_1, \omega_2, \omega_3)$ being used to relate velocity to a known, imposed force and $\hat{\zeta}_1(\omega)$ and $\hat{\zeta}_3(\omega_1, \omega_2, \omega_3)$ being used to relate force to a known, imposed velocity. Thus, the force and velocity can be very generally represented as

$$\begin{aligned}
 \hat{F}(\omega) &= \zeta_1(\omega)\hat{v}(\omega) \\
 &\quad + \iint\int_{-\infty}^{\infty} \zeta_3(\omega_1, \omega_2, \omega_3)\delta(\omega - \omega_1 - \omega_2 - \omega_3) \\
 &\quad \times \hat{v}(\omega_1)\hat{v}(\omega_2)\hat{v}(\omega_3)d\omega_1d\omega_2d\omega_3,
 \end{aligned}
 \tag{B4}$$

$$\begin{aligned}
 \hat{v}(\omega) &= \hat{\zeta}_1(\omega)\hat{F}(\omega) \\
 &\quad + \iint\int_{-\infty}^{\infty} \hat{\zeta}_3(\omega_1, \omega_2, \omega_3)\delta(\omega - \omega_1 - \omega_2 - \omega_3) \\
 &\quad \times \hat{F}(\omega_1)\hat{F}(\omega_2)\hat{F}(\omega_3)d\omega_1d\omega_2d\omega_3.
 \end{aligned}
 \tag{B5}$$

where, for example, in this case the leading-order transfer function $\zeta_1(\omega) = 6\pi\eta^*(\omega)$; this can be seen by inspection of Eq. (20).

The transfer functions $\zeta_1(\omega)$, $\zeta_3(\omega_1, \omega_2, \omega_3)$ and $\hat{\zeta}_1(\omega)$, $\hat{\zeta}_3(\omega_1, \omega_2, \omega_3)$ can be related to one another through the following method, and thus used to invert the force-velocity relationships in Eqs. (34) and (A1) and calculate the velocity resulting from a known, imposed force.

First, the force and velocity are both expanded as a power series in some small parameter ϵ , which to second order take the form

$$\hat{F}(\omega) = \hat{F}_0 + \epsilon^2\hat{F}_2 + O(\epsilon^4),
 \tag{B6a}$$

$$\hat{v}(\omega) = \hat{v}_0 + \epsilon^2\hat{v}_2 + O(\epsilon^4),
 \tag{B6b}$$

where only $\mathcal{O}(\epsilon)$ and $\mathcal{O}(\epsilon^2)$ terms are retained, as no non-zero terms are expected at $\mathcal{O}(\epsilon^1)$.

Substituting the expansions of \hat{F} and \hat{v} in Eqs. (B4) and (B5) into the representation of velocity \hat{v} in Eq. (B6b) and retaining only terms up to order $\mathcal{O}(\epsilon^2)$ yields the following expression:

$$\begin{aligned}
 \hat{v}_0 + \epsilon^2\hat{v}_2 &= \zeta_1(\omega)\zeta_1(\omega)\hat{v}_0(\omega) + \epsilon^2\zeta_1(\omega)\zeta_1(\omega)\hat{v}_2(\omega) \\
 &\quad + \epsilon^2\zeta_1(\omega) \iint\int_{-\infty}^{\infty} \zeta_3(\omega_1, \omega_2, \omega_3)\delta(\omega - \sum_i \delta(\omega_i)) \\
 &\quad \times \hat{v}_0(\omega_1)\hat{v}_0(\omega_2)\hat{v}_0(\omega_3)d\omega_1d\omega_2d\omega_3 \\
 &\quad + \epsilon^2 \iint\int_{-\infty}^{\infty} \hat{\zeta}_3(\omega_1, \omega_2, \omega_3)\hat{\zeta}_1(\omega_1)\hat{\zeta}_1(\omega_2)\hat{\zeta}_1(\omega_3) \\
 &\quad \times \delta(\omega - \sum_i \delta(\omega_i))\hat{v}_0(\omega_1)\hat{v}_0(\omega_2)\hat{v}_0(\omega_3)d\omega_1d\omega_2d\omega_3.
 \end{aligned}
 \tag{B7}$$

Matching the terms at leading order in ϵ , or $\mathcal{O}(1)$, gives a simple relationship between $\zeta_1(\omega)$ and $\hat{\zeta}_1(\omega)$,

$$\hat{\zeta}_1(\omega) = \frac{1}{\zeta_1(\omega)}.
 \tag{B8}$$

Matching terms at order $\mathcal{O}(\epsilon^2)$ can be simplified as

$$\begin{aligned}
 &-\frac{1}{\zeta_1(\omega)} \iint\int_{-\infty}^{\infty} \zeta_3(\omega_1, \omega_2, \omega_3)\delta(\omega - \sum_i \delta(\omega_i)) \\
 &\quad \times \hat{v}_0(\omega_1)\hat{v}_0(\omega_2)\hat{v}_0(\omega_3)d\omega_1d\omega_2d\omega_3 \\
 &= \iint\int_{-\infty}^{\infty} \zeta_3(\omega_1, \omega_2, \omega_3)\hat{\zeta}_1(\omega_1)\hat{\zeta}_1(\omega_2)\hat{\zeta}_1(\omega_3) \\
 &\quad \times \delta(\omega - \sum_i \delta(\omega_i))\hat{v}_0(\omega_1)\hat{v}_0(\omega_2)\hat{v}_0(\omega_3)d\omega_1d\omega_2d\omega_3,
 \end{aligned}
 \tag{B9}$$

which, using the sifting property of the delta function, can be re-expressed with $\zeta(\omega)$ moved inside the first integral

$$\begin{aligned}
 &-\iint\int_{-\infty}^{\infty} \frac{\zeta_3(\omega_1, \omega_2, \omega_3)}{\zeta_1(\omega_1 + \omega_2 + \omega_3)}\delta(\omega - \sum_i \delta(\omega_i)) \\
 &\quad \times \hat{v}_0(\omega_1)\hat{v}_0(\omega_2)\hat{v}_0(\omega_3)d\omega_1d\omega_2d\omega_3 \\
 &= \iint\int_{-\infty}^{\infty} \zeta_3(\omega_1, \omega_2, \omega_3)\hat{\zeta}_1(\omega_1)\hat{\zeta}_1(\omega_2)\hat{\zeta}_1(\omega_3)\delta(\omega - \sum_i \delta(\omega_i)) \\
 &\quad \times \hat{v}_0(\omega_1)\hat{v}_0(\omega_2)\hat{v}_0(\omega_3)d\omega_1d\omega_2d\omega_3.
 \end{aligned}
 \tag{B10}$$

Comparing the forms of these integrals, we can find the final expression for $\hat{\zeta}_3(\omega_1, \omega_2, \omega_3)$

$$\hat{\zeta}_3(\omega_1, \omega_2, \omega_3) = \frac{\zeta_3(\omega_1, \omega_2, \omega_3)}{\zeta_1(\omega_1 + \omega_2 + \omega_3)\zeta_1(\omega_1)\zeta_1(\omega_2)\zeta_1(\omega_3)}.
 \tag{B11}$$

Using this method, we can express a second-order contribution to the velocity of particle subjected to a known external force $\hat{F}(\omega) = \hat{F}_1(\omega)\mathbf{e}_1 + \hat{F}_2(\omega)\mathbf{e}_2$ arising from translation-rotation coupling

$$\begin{aligned}
 \hat{v}_2 &= \frac{1}{(2\pi)^2}\mathbf{e}_1 \iint\int_{-\infty}^{\infty} H_1(\omega_1, \omega_2, \omega_3)[\hat{F}_2(\omega_1)\hat{F}_2(\omega_2)\hat{V}_1(\omega_3) \\
 &\quad - \hat{F}_2(\omega_1)\hat{V}_1(\omega_2)\hat{F}_2(\omega_3)]d\omega_1d\omega_2d\omega_3 \\
 &\quad - \frac{1}{(2\pi)^2}\mathbf{e}_1 \iint\int_{-\infty}^{\infty} H_2(\omega_1, \omega_2, \omega_3)[\hat{F}_2(\omega_1)\hat{F}_1(\omega_2)\hat{F}_2(\omega_3) \\
 &\quad - \hat{F}_1(\omega_1)\hat{F}_2(\omega_2)\hat{F}_2(\omega_3)]d\omega_1d\omega_2d\omega_3 \\
 &\quad + \frac{1}{(2\pi)^2}\mathbf{e}_2 \iint\int_{-\infty}^{\infty} H_1(\omega_1, \omega_2, \omega_3)[\hat{F}_1(\omega_1)\hat{F}_2(\omega_2)\hat{F}_1(\omega_3) \\
 &\quad - \hat{F}_1(\omega_1)\hat{F}_1(\omega_2)\hat{F}_2(\omega_3)]d\omega_1d\omega_2d\omega_3 \\
 &\quad - \frac{1}{(2\pi)^2}\mathbf{e}_2 \iint\int_{-\infty}^{\infty} H_2(\omega_1, \omega_2, \omega_3)[\hat{F}_2(\omega_1)\hat{V}_1(\omega_2)\hat{V}_1(\omega_3) \\
 &\quad - \hat{F}_1(\omega_1)\hat{F}_2(\omega_2)\hat{F}_1(\omega_3)]d\omega_1d\omega_2d\omega_3,
 \end{aligned}
 \tag{B12}$$

where the kernel functions in Eq. (B11) are given by

$$\begin{aligned}
 H_1(\omega_1, \omega_2, \omega_3) &= -\frac{K_1(\omega_1, \omega_2, \omega_3)}{N_1(\omega_1 + \omega_2 + \omega_3)N_1(\omega_1)N_1(\omega_2)N_1(\omega_3)}, \\
 H_2(\omega_1, \omega_2, \omega_3) &= -\frac{K_2(\omega_1, \omega_2, \omega_3)}{N_1(\omega_1 + \omega_2 + \omega_3)N_1(\omega_1)N_1(\omega_2)N_1(\omega_3)},
 \end{aligned}$$

where $K_1(\omega_1, \omega_2, \omega_3)$ and $K_2(\omega_1, \omega_2, \omega_3)$ are defined in Eq. (B3) and $N_1(\omega)\zeta_1(\omega) = 6\pi\eta^*(\omega)$, per Eq. (20). The same inversion rationale can be applied to the purely translational component of the force-velocity relationship in Eq. (A1) as well, allowing calculation of the trajectory components arising from purely translational forces.

REFERENCES

- ¹G. H. McKinley, "Steady transient motion of spherical particles in viscoelastic liquids," in *Transport Processes in Bubbles, Drops and Particles*, 2nd ed., edited by E. Chhabra and D. D. Kee (Taylor & Francis, 2001).
- ²E. S. G. Shaqfeh, "On the rheology of particle suspensions in viscoelastic fluids," *AIChE J.* **65**, e16575 (2019).
- ³R. I. Tanner, "Computation and experiment in non-colloidal suspension rheology," *J. Non-Newtonian Fluid Mech.* **281**, 104282 (2020).
- ⁴K. Zhao and T. G. Mason, "Assembly of colloidal particles in solution," *Rep. Prog. Phys.* **81**, 126601 (2018).
- ⁵L. E. Becker, G. H. McKinley, H. K. Rasmussen, and O. Hassager, "The unsteady motion of a sphere in a viscoelastic fluid," *J. Rheol.* **38**, 377–403 (1994).
- ⁶K. D. Housiadas and R. I. Tanner, "A high-order perturbation solution for the steady sedimentation of a sphere in a viscoelastic fluid," *J. Non-Newtonian Fluid Mech.* **233**, 166–180 (2016).
- ⁷K. D. Housiadas and R. I. Tanner, "The angular velocity of a freely rotating sphere in a weakly viscoelastic matrix fluid," *Phys. Fluids* **23**, 051702 (2011).
- ⁸A. Castillo, W. L. Murch, J. Einarsson, B. Mena, E. S. G. Shaqfeh, and R. Zenit, "Drag coefficient for a sedimenting and rotating sphere in a viscoelastic fluid," *Phys. Rev. Fluids* **4**, 1–22 (2019).
- ⁹F. Snijkers, G. D'Avino, P. L. Maffettone, F. Greco, M. A. Hulsen, and J. Vermant, "Effect of viscoelasticity on the rotation of a sphere in shear flow," *J. Non-Newtonian Fluid Mech.* **166**, 363–372 (2011).
- ¹⁰G. D'Avino, M. A. Hulsen, F. Snijkers, J. Vermant, F. Greco, and P. L. Maffettone, "Rotation of a sphere in a viscoelastic liquid subjected to shear flow. Part I: Simulation results," *J. Rheol.* **52**, 1331–1346 (2008).
- ¹¹K. D. Housiadas and R. I. Tanner, "Perturbation solution for the viscoelastic 3D flow around a rigid sphere subject to simple shear," *Phys. Fluids* **23**, 083101 (2011).
- ¹²H. Giesekus, "Strömungen mit konstantem Geschwindigkeitsgradienten und die Bewegung von darin suspendierten Teilchen—Teil I: Räumliche Strömungen," *Rheol. Acta* **2**, 101–112 (1962).
- ¹³H. Giesekus, "Die simultane Translations- und Rotationsbewegung einer Kugel in einer elastoviskosen Flüssigkeit," *Rheol. Acta* **3**, 59–71 (1963).
- ¹⁴F. M. Leslie and R. I. Tanner, "The slow flow of a viscoelastic liquid past a sphere," *Q. J. Mech. Appl. Math.* **14**, 36–48 (1961).
- ¹⁵R. I. Tanner and K. Walters, "Hanswalter Giesekus 1922–2017," *Rheol. Acta* **57**, 691–692 (2018).
- ¹⁶H. Giesekus, "Die Elastizität von Flüssigkeiten," *Rheol. Acta* **5**, 29–35 (1966).
- ¹⁷H. Giesekus, "A simple constitutive equation for polymer fluids based on the concept of deformation-dependent tensorial mobility," *J. Non-Newtonian Fluid Mech.* **11**, 69–109 (1982).
- ¹⁸R. B. Bird, R. C. Armstrong, and O. Hassanger, *Dynamics of Polymeric Liquids, Volume 1: Fluid Mechanics*, 2nd ed. (Wiley, 1987).
- ¹⁹M. A. Hulsen and J. van der Zanden, "Numerical simulation of contraction flows using a multi-mode Giesekus model," *J. Non-Newtonian Fluid Mech.* **38**, 183–221 (1991).
- ²⁰X. Su, Z. Xu, Z. Wang, H. Jin, S. Wu, and Y. Lu, "Data-driven closure model for the drag coefficient of the creeping flow past a translating sphere in a shear-thinning viscoelastic fluid," *Powder Technol.* **400**, 117266 (2022).
- ²¹L. M. Quinzani, G. H. McKinley, R. A. Brown, and R. C. Armstrong, "Modeling the rheology of polyisobutylene solutions," *J. Rheol.* **34**, 705–748 (1990).
- ²²J. P. Rothstein, "Transient extensional rheology of wormlike micelle solutions," *J. Rheol.* **47**, 1227 (2003).
- ²³M. T. Arigo and G. H. McKinley, "An experimental investigation of negative wakes behind spheres settling in a shear-thinning viscoelastic fluid," *Rheol. Acta* **37**, 307–327 (1998).
- ²⁴M. D. Torres, B. Hallmark, L. Hilliu, and D. I. Wilson, "Natural Giesekus fluids: Shear and extensional behavior of food gum solutions in the semi-dilute regime," *AIChE J.* **60**, 3902–3915 (2014).
- ²⁵S. Varchanis, Y. Dimakopoulos, C. Wagner, and J. Tsamopoulos, "How viscoelastic is human blood plasma?," *Soft Matter* **14**, 4238–4251 (2018).
- ²⁶Z. Li and J. Lin, "On the some issues of particle motion in the flow of viscoelastic fluids," *Acta Mech. Sin.* **38**, 321467 (2022).
- ²⁷S. Dai and R. I. Tanner, "Rheology of non-colloidal suspensions with viscoelastic matrices," *Soft Matter* **16**, 9519–9524 (2020).
- ²⁸M. D. Chilcott and J. H. Rallison, "Creeping flow of dilute polymer solutions past cylinders and spheres," *J. Non-Newtonian Fluid Mech.* **29**, 381–432 (1988).
- ²⁹C. Bodart and M. J. Crochet, "The time-dependent flow of a viscoelastic fluid around a sphere," *J. Non-Newtonian Fluid Mech.* **54**, 303–329 (1994).
- ³⁰M. N. J. Moore and M. J. Shelley, "A weak-coupling expansion for viscoelastic fluids applied to dynamic settling of a body," *J. Non-Newtonian Fluid Mech.* **183–184**, 25–36 (2012).
- ³¹M. A. Joens and J. W. Swan, "Unsteady and lineal translation of a sphere through a viscoelastic fluid," *Phys. Rev. Fluids* **7**, 013301 (2022).
- ³²D. Son, M. C. Ugurlu, and M. Sitti, "Permanent magnet array-driven navigation of wireless millirobots inside soft tissues," *Sci. Adv.* **7**, 1–11 (2021).
- ³³J. G. Lee, A. M. Brooks, W. A. Shelton, K. J. M. Bishop, and B. Bharti, "Directed propulsion of spherical particles along three dimensional helical trajectories," *Nat. Commun.* **10**, 2575 (2019).
- ³⁴Z. Ye and M. Sitti, "Dynamic trapping and two-dimensional transport of swimming microorganisms using a rotating magnetic microrobot," *Lab Chip* **14**, 2177–2182 (2014).
- ³⁵S. K. Gupta, J. Sun, Y. L. Han, C. Lyu, T. He, and M. Guo, "Quantification of Cell-Matrix interaction in 3D using optical tweezers," in *Multi-Scale Extracellular Matrix Mechanics and Mechanobiology*, edited by Y. Zhang (Springer International Publishing, Cham, 2020), pp. 283–310.
- ³⁶A. Spatafora-Salazar, L. H. P. Cunha, and S. L. Biswal, "Periodic deformation of semiflexible colloidal chains in eccentric time-varying magnetic fields," *J. Phys.: Condens. Matter* **34**, 184005 (2022).
- ³⁷L. W. Rogowski, J. Ali, X. Zhang, J. N. Wilking, H. C. Fu, and M. J. Kim, "Symmetry breaking propulsion of magnetic microspheres in nonlinearly viscoelastic fluids," *Nat. Commun.* **12**, 1116 (2021).
- ³⁸L. A. Kroo, J. P. Binagia, N. Eckman, M. Prakash, and E. S. G. Shaqfeh, "A freely suspended robotic swimmer propelled by viscoelastic normal stresses," *J. Fluid Mech.* **944**, A20 (2022).
- ³⁹R. Schuech, R. Cortez, and L. Fauci, "Performance of a helical microswimmer traversing a discrete viscoelastic network with dynamic remodeling," *Fluids* **7**, 257 (2022).
- ⁴⁰R. J. Poole, "The Deborah and Weissenberg numbers," *Br. Soc. Rheol.* **53**, 32–39 (2012).
- ⁴¹J. M. Dealy, "Weissenberg and Deborah numbers—Their definition and use," *Rheol. Bull.* **79**, 14–19 (2010).
- ⁴²H. Masoud and H. A. Stone, "The reciprocal theorem in fluid dynamics and transport phenomena," *J. Fluid Mech.* **879**, P1 (2019).
- ⁴³B. Schnurr, F. Gittes, F. C. MacKintosh, and C. F. Schmidt, "Determining microscopic viscoelasticity in flexible and semiflexible polymer networks from thermal fluctuations," *Macromolecules* **30**, 7781–7792 (1997).
- ⁴⁴E. Guazzelli and J. F. Morris, *A Physical Introduction to Suspension Dynamics* (Cambridge University Press, New York, 2012).
- ⁴⁵S. A. Klioner, "New system for indicial computation and its applications in gravitational physics," *Comput. Phys. Commun.* **115**, 231–244 (1998).
- ⁴⁶S. K. Gupta, K. R. Lennon, M. A. Joens, H. Bandi, M. Van Galen, Y. Han, W. Tang, Y. Li, S. C. Wasserman, J. W. Swan, and M. Guo, "Optical tweezer measurements of asymptotic nonlinearities in complex fluids," *Phys. Rev. E* **104**, 064604 (2021).
- ⁴⁷K. R. Lennon, G. H. McKinley, and J. W. Swan, "Medium amplitude parallel superposition (MAPS) rheology. Part I: Mathematical framework and theoretical examples," *J. Rheol.* **64**, 551–579 (2020).